Dating continental subduction beneath the Samail Ophiolite: garnet, zircon, and rutile petrochronology of the As Sifah eclogites, NE Oman

Joshua M. Garber[1,*], Matthew Rioux[2,3], Michael P. Searle[4], Andrew R.C. Kylander-Clark[2,3], Bradley R. Hacker[2,3], Jeff D. Vervoort[5], Clare J. Warren[6], Andrew J. Smye[1]

[1]Department of Geosciences, The Pennsylvania State University
[2]Department of Earth Science, University of California Santa Barbara
[3]Earth Research Institute, University of California Santa Barbara
[4]Department of Earth Sciences, Oxford University
[5]School of the Environment, Washington State University
[6]School of Environment, Earth and Ecosystem Sciences, The Open University, Walton Hall, Milton Keynes MK7 6AA

*corresponding author: Joshua M. Garber (jxg1395@psu.edu) [ORCID: 0000-0001-5313-0982]

Key Points:

- Sm-Nd garnet, U-Pb zircon, and U-Pb rutile dates from As Sifah cluster from ~81–77 Ma
- All data suggest NE-dipping subduction of the Arabian continental margin beneath the already-obducted Samail Ophiolite
- Deep subduction and exhumation of the Arabian margin occurred more slowly than most other *HP* settings

ABSTRACT

Studies of the high-pressure (*HP*) As Sifah eclogites in the NE part of the Saih Hatat window, Oman, have used different radiometric dating results (Ar/Ar, Sm-Nd *vs.* U-Pb, Rb-Sr) to interpret disparate tectonic models for the timing, geometry, and cause of continental subduction – including its association with the Samail Ophiolite. To determine the absolute timing of continental subduction, we coupled geochronological and geochemical analyses of major (garnet) and accessory phases (zircon, rutile) from the highest-grade metamorphic rocks in the Saih Hatat (As Sifah eclogites). Early Permian (283.8±0.7 Ma) tuffaceous zircon cores are consistent with earlier interpretations that the As Sifah rocks were sourced from a distal portion of the Arabian continental margin. Data from a range of bulk compositions, metamorphic assemblages, and rock textures consistently suggest a single metamorphic event, with garnet growth starting by ~81 Ma and ceasing by ~77 Ma, with slight but consistent offsets in the timing of metamorphic (re)crystallization between different lithologies. These new data confirm previous structural, metamorphic, and geochronological interpretations for continental *HP* metamorphism in a single NE-dipping subduction zone beneath the already obducted Samail Ophiolite; there is no robust evidence for a ~110 Ma event or a continental-ward dipping subduction zone. Combined with literature constraints, our data suggest that the As Sifah unit was subducted and exhumed relatively slowly (~5 mm/yr) compared to other continental high-pressure settings – likely associated with the dragging to mantle depths by a mafic root, followed by long residence in the lower to middle crust.

PLAIN TEXT SUMMARY

The subduction of continental material to mantle depths is of interest because **i**) it is associated with the recycling of surface material to the deep mantle and **ii**) these types of rocks have been exhumed to the Earth’s surface almost exclusively since <1.0 Ga. The Saih Hatat window, Oman, is a unique expression of this process where buoyant continent material apparently subducted and exhumed beneath a denser ophiolite (slice of oceanic crust and mantle). However, the timing and geometry of this process has been controversial. We measured isotopic dates and trace elements from several different phases in a suite of

representative samples from the highest-grade metamorphic rocks, and found that each gave the same range of dates (~81–77 Ma). There are small variations due to changes in bulk composition, but our data firmly suggest a single subduction metamorphism episode. These results require the subduction of the Arabian continental margin after the obduction of the Samail Ophiolite, and suggest that the most deeply subducted, most outboard continental margin rocks were anchored to a dense mafic root before detaching and eventually penetrating upwards through the ophiolite.

1 INTRODUCTION

High to ultra-high pressure (*HP-UHP*) continental subduction is a well-documented process that appears to be a hallmark of plate tectonics at least since the Neoproterozoic. Exposed examples of continental subduction beneath continental upper plates show consistent trends in their rates of subduction and exhumation from the mantle, primarily based on their size, orogenic stage, and bulk composition [*Kylander-Clark et al.*, 2012; *Young and Kylander-Clark*, 2015]. In contrast, continental subduction beneath oceanic crust is rare, and is typically observed in association with recent (<100 Ma) ophiolite obduction, including in New Caledonia and Oman [e.g., *Agard and Vitale-Brovarone*, 2013]. This style of continental subduction occurs under some of the coldest modern metamorphic geotherms [*Agard and Vitale-Brovarone*, 2013; *Vitale Brovarone and Agard*, 2013; *Agard et al.*, 2018], contrasting with the ultra-high metamorphic temperatures (*T*=800–900°C) attained during sole metamorphism at the base of ophiolites that now structurally overlie these *HP* rocks [*Hacker and Mosenfelder*, 1996; *Searle and Cox*, 2002; *Dewey and Casey*, 2013; *Cowan et al.*, 2014; *Agard et al.*, 2016; *Soret et al.*, 2017].

The northern part of the Saih Hatat window of NE Oman (Figure 1) is the best-exposed example of this type of *HP* continental orogen, but the sequence of tectonic events leading to continental subduction is controversial. Contrasting geochronology on the structurally lowest, highest-grade metamorphic rocks in the Saih Hatat, at As Sifah beach [P>2.0 GPa, T>530°C: *Searle et al.*, 1994; *Warren and Waters*, 2006; *Massonne et al.*, 2013], has led to two entirely different interpretations for the timing and geometry of subduction. Based on Ar/Ar mica dates and Sm-Nd garnet-WR isochron dates

[*Montigny et al.*, 1988; *El-Shazly and Lanphere*, 1992; *Miller et al.*, 1999; *Gray et al.*, 2004a; *Gray et al.*, 2004b; *Goscombe et al.*, 2020] as well as structural arguments [*Miller et al.*, 1998; *Miller et al.*, 2002], one model suggests that the deeply subducted As Sifah rocks are polymetamorphic, with a prograde metamorphic episode around ~130–110 Ma and exhumation-related metamorphism at ~80 Ma. This model has also been suggested in the context of continental subduction to the SW, i.e., toward the Arabian margin [e.g., *Gregory et al.*, 1998; *Gray and Gregory*, 2000; *Goscombe et al.*, 2020]. A separate set of studies, based on U-Pb zircon and Rb-Sr isochron dating [*El-Shazly et al.*, 2001; *Warren et al.*, 2003; *Searle et al.*, 2004; *Warren et al.*, 2005] but also supported by structural, metamorphic, and stratigraphic studies [*Goffé et al.*, 1988; *El-Shazly et al.*, 1990; *Searle et al.*, 1994; *Searle and Cox*, 1999; 2002; *Searle et al.*, 2004; *Warren and Miller*, 2007], suggests a single metamorphic episode for the As Sifah rocks at ~80 Ma during subduction to the NE, away from the Arabian margin. Because this episode would immediately postdate and match the polarity of subduction beneath the Samail Ophiolite [*Searle et al.*, 2004; *Searle*, 2007; *Cowan et al.*, 2014; *Rioux et al.*, 2016], this interpretation suggests that continental subduction arose as part of the same process driving ophiolite formation and obduction [a case numerically modeled by *Duretz et al.*, 2016]. In this case, all older Ar/Ar and Sm-Nd dates must be erroneous. This is not particularly controversial for the Ar/Ar dates, because extraneous Ar has been repeatedly shown to be a problem in *HP* metamorphic rocks in general and the As Sifah eclogites in particular [*El-Shazly et al.*, 2001; *Warren et al.*, 2011; *Smye et al.*, 2013].

There is little dispute that the uppermost, low-grade continental nappes in the Saih Hatat region preserve only a single-stage metamorphic history related to ophiolite obduction onto the margin at ~80 Ma [e.g., *El-Shazly and Lanphere*, 1992]. Additionally, different authors have used the same structural and metamorphic observations from the deeper, high-grade portions of the Saih Hatat window in support of either a single-stage [*El-Shazly et al.*, 1990; *Searle et al.*, 2004; *Warren and Miller*, 2007] or polymetamorphic history [*Miller et al.*, 1999; *Gray et al.*, 2004a; *Gray et al.*, 2004b; *Goscombe et al.*, 2020]. The controversy thus hinges entirely on the timing and duration of metamorphism in the lowermost rocks, particularly how Sm-Nd and U-Pb dates relate to growth of rock-forming metamorphic phases. Therefore, to understand the timing of metamorphism in the most deeply subducted rocks in the Saih Hatat, we performed new high-resolution garnet, zircon, and rutile isotopic (Sm-Nd, U-Pb) and trace-element measurements on the As Sifah eclogites. These data provide robust new constraints on the timing of subduction metamorphism and the protolith character of the subducted rocks; they also provide a unique comparison between the metamorphic, isotopic, and geochemical records in different endmember bulk compositions during the same event. We conclude by comparing our data to other *(U)HP* orogens globally to understand the unique tectonic character of continental subduction beneath ophiolites.

2 GEOLOGIC BACKGROUND

The Saih Hatat window (NE Oman) records the collapse, partial subduction, and exhumation of the Arabian continental margin, the latter stages of which correlate with the emplacement of the Samail Ophiolite [*Lippard*, 1983; *Michard*, 1983; *Le Metour et al.*, 1986; *Goffé et al.*, 1988; *El-Shazly et al.*, 1990; *El-Shazly and Coleman*, 1990; *Le Métour et al.*, 1990; *Michard et al.*, 1991; *El-Shazly and Lanphere*, 1992; *Michard et al.*, 1994; *Searle et al.*, 1994; *Gregory et al.*, 1998; *Jolivet et al.*, 1998; *El-Shazly et al.*, 2001; *Warren et al.*, 2003; *Gray et al.*, 2004a; *Gray et al.*, 2004b; *Searle et al.*, 2004; *Warren et al.*, 2005; *Searle*, 2007; *Warren and Miller*, 2007; *Yamato et al.*, 2007; *Agard et al.*, 2010b; *Duretz et al.*, 2016]. This record is expressed as a domed series of stacked, metamorphosed (high-*P*/low-*T*), fault- or shear-zone-bounded units exposed in a structural window through the obducted Samail Ophiolite (**Fig. 1a**). The rocks are multiply deformed, but the primary penetrative structural features are top-to-the-NNE fabrics related to exhumation of footwall rocks to the southwest [*Miller et al.*, 2002; *Gray et al.*, 2004b; *Searle et al.*, 2004; *Agard et al.*, 2010b], which is associated with the timing of peak to retrograde metamorphism [*El-Shazly et al.*, 1990; *El-Shazly et al.*, 1997; *Warren et al.*, 2003]. The stratigraphy of most of the Saih Hatat is similar to the Precambrian to Cretaceous continental margin sequence exposed elsewhere in the Oman Mountains, including the Jebel Akhdar window to the west [e.g., *Glennie et al.*, 1973; *Mann and Hanna*, 1990; *Chauvet et al.*, 2009], permitting detailed structural reconstructions [*Miller et al.*, 2002; *Searle et al.*, 2004; *Warren and Miller*, 2007].

The most deeply subducted rocks in the Saih Hatat (**Fig. 1b**) occur in two exposures beneath a major shear zone that has been termed the Upper Plate-Lower Plate (UP-LP) discontinuity [*Gregory et al.*, 1998; *Miller et al.*, 1998; *Miller et al.*, 2002] or the Hulw Detachment [*Searle et al.*, 2004; 2005], although similar *P-T* conditions above and below the structure suggest that it is not a lithosphere-scale feature [*Searle et al.*, 2004; *Gray et al.*, 2005b; *Searle et al.*, 2005; *Yamato et al.*, 2007; *Agard et al.*, 2010a]. In the westernmost exposure (Hulw Window), the UP-LP discontinuity separates rocks that show near-identical peak metamorphic *P* on either side (~1.0 GPa) and little variation in *T*, either across the discontinuity or within the window itself [*Yamato et al.*, 2007; *Agard et al.*, 2010b]. However, there is a major increase in deformation intensity toward the shear zone in the upper plate [*Miller et al.*, 2002]. The easternmost As Sifah Window exhibits a stratigraphic sequence matching the Hulw Window [*Miller et al.*, 2002; *Warren and Miller*, 2007], but with significantly higher peak metamorphic pressures and temperatures ($P \leq 2.5$ GPa, T=550–600°C) [*Searle et al.*, 1994; *Warren and Waters*, 2006; *Yamato et al.*, 2007; *Massonne et al.*, 2013]. Unlike the Hulw Window, the As Sifah Window shows an apparent increase in metamorphic grade to the NNE [*Searle et al.*, 2004; *Yamato et al.*, 2007], although this may also reflect different extents of retrogression [*Warren and Waters*, 2006]. Highly attenuated isoclinal folds in both windows are cut by the UP-LP discontinuity, suggesting that the As Sifah rocks were exhumed to the same depth as the Hulw Window prior to mostly lateral motion along the shear zone [*Miller et al.*, 2002; *Gray et al.*, 2004b; *Searle et al.*, 2004; *Warren and Miller*, 2007].

The structurally lowest, highest-grade metamorphic rocks in the Saih Hatat are exposed in metavolcanic lenses along the coast ~1–2 km north of the village of As Sifah (**Fig. 1b**). The lithologic horizon in which the highest-grade assemblages occur is recognizable and traceable through the entirety of the Hulw and As Sifah Windows [units Lvm and Lvf on Fig. 1b: *Miller et al.*, 2002; *Gray et al.*, 2005a; *Warren and Miller*, 2007; *Chauvet et al.*, 2009], but they only contain eclogite-facies assemblages within a few km of coast [*Searle et al.*, 1994; *Searle et al.*, 2004; *Warren and Waters*, 2006]. A SHRIMP U-Pb zircon date from a felsic metatuff at As Sifah suggested that this horizon represents late Carboniferous (~298 Ma) volcanic flows and tuffs associated with the breakup of Pangaea [*Gray et al.*, 2005a], which is slightly older than the timing of extension recorded elsewhere in Oman [*Angiolini et al.*, 2003]. Still, this date fits within other "lower-plate" stratigraphic constraints: quartz-mica schists underlying the boudins have been correlated with the Ordovician Amdeh Formation, whereas calc-schists above may represent the Permian Saiq Formation [*Miller et al.*, 2002; *Searle et al.*, 2004; *Warren and Miller*, 2007], suggesting that the As Sifah beach exposure represents an outboard subducted remnant of the pre-Permian unconformity observed throughout NE Oman. Most workers thus conclude that the As Sifah and Hulw Windows reflect a more distal part of the same Arabian margin sequence exposed in structurally higher, lower-grade units [*Searle et al.*, 2004; *Warren and Miller*, 2007; *Chauvet et al.*, 2009], while others have suggested they are the remnants of an outboard microplate [*Gray and Gregory*, 2000; *Gray et al.*, 2004b; *Gray et al.*, 2005a].

Our sampling location (As Sifah beach; see **Fig. 1b**) is described in detail elsewhere, including *Searle et al.* [2004, their Fig. 7] and *Gray et al.* [2004b, their Fig. 7]. The outcrop is a lens of foliated to granoblastic mafic garnet blueschists and eclogites, with less-common (but still eclogite-facies) schistose felsic layers; this mafic lens is enclosed by metacarbonates and calcschists, and crosscut by quartz-hematite veins [*El-Shazly et al.*, 1990; *Searle et al.*, 1994; *El-Shazly et al.*, 1997; *El-Shazly*, 2001; *Gray et al.*, 2004a; *Gray et al.*, 2004b; *Searle et al.*, 2004; *Gray et al.*, 2005a; *Warren and Waters*, 2006; *Massonne et al.*, 2013]. Phase equilibria and elastic inclusion relationships suggest peak *P-T* conditions of ~2.5 GPa and ~550°C [*Wendt et al.*, 1993; *Searle et al.*, 1994; *Warren and Waters*, 2006; *Massonne et al.*, 2013], although others argue for lower peak pressures [<15 kbar: *El-Shazly*, 2001]. All rocks reached peak conditions along clockwise P-T paths and relatively cold geotherms [*El-Shazly et al.*, 1990; *El-Shazly and Coleman*, 1990] that are variably recorded by different bulk compositions [*El-Shazly et al.*, 1997]. Some rocks contain relict prograde minerals as inclusions in garnet cores (including lawsonite pseudomorphs, epidote, and chloritoid), whereas other rocks contain garnets with only peak to early retrograde metamorphic phases like rutile, phengite, blue amphibole, and omphacitic or jadeitic pyroxene

[*El-Shazly and Liou*, 1991; *El-Shazly et al.*, 1997; *Gray et al.*, 2004a; *Gray et al.*, 2004b; *Warren and Waters*, 2006; *Massonne et al.*, 2013]. Most mafic rocks, particularly those that suffered fluid ingress [*El-Shazly et al.*, 1997], have been affected by a late retrograde overprint to an epidote-albite-green amphibole-chlorite assemblage, suggesting slight heating during retrogression [e.g., *El-Shazly et al.*, 1990; *Gray et al.*, 2004b; *Massonne et al.*, 2013]. There is no existing mineralogical or garnet chemical zoning evidence for distinct metamorphic stages, nor for a pause between different garnet growth episodes [e.g., *Warren and Waters*, 2006].

As noted above, there is a long and controversial history of geochronology from the As Sifah rocks (**Fig. 2**). On the basis of K-Ar white mica ages spanning ~130–80 Ma in the Hulw and As Sifah windows, as well as $^{40}Ar/^{39}Ar$ step heating experiments, *Montigny et al.* [1988] reasoned that the *HP* metamorphic history of As Sifah could have involved **i**) two distinct metamorphic events, one at ~130–110 Ma and the other at ~80 Ma, or **ii**) a single metamorphic episode at ~80 Ma, with older dates resulting from extraneous Ar. A similar conclusion (distinct ~110 and 80 Ma *HP* metamorphic episodes) was reached by *El-Shazly and Lanphere* [1992] based on additional $^{40}Ar/^{39}Ar$ data; however, subsequent Rb-Sr isochron dating led the same group to interpret that all older $^{40}Ar/^{39}Ar$ dates result from extraneous Ar and all metamorphism occurred solely at ~80 Ma [*El-Shazly et al.*, 2001]. This contention was subsequently strengthened by TIMS U-Pb zircon and rutile ages of ~79–78 Ma [*Warren et al.*, 2003; *Warren et al.*, 2005], each of which occurs as inclusions in the major rock-forming phases – suggesting peak metamorphism at that time.

In contrast, *Gray et al.* [2004a] dated eclogite-facies assemblages in the As Sifah Window to 110±9 Ma and 109±13 Ma using Sm-Nd garnet-whole rock (WR) isochrons, and suggested that these represented the timing of peak *HP* metamorphism; a younger SHRIMP U-Pb zircon date at ~82 Ma (as well as earlier U-Pb and Rb-Sr dates, and a secondary Sm-Nd isochron date) were suggested to record exhumation. Further $^{40}Ar/^{39}Ar$ dating of different generations of white micas [*Miller et al.*, 1999; *Gray et al.*, 2004b] in combination with detailed structural mapping [*Miller et al.*, 1998; *Miller et al.*, 2002] were used to suggest that As Sifah underwent prograde southward subduction at ~120–110 Ma and retrograde exhumation at ~80 Ma [*Miller et al.*, 1998; *Miller et al.*, 1999; *Miller et al.*, 2002; *Gray et al.*, 2004b]. High-precision laser $^{40}Ar/^{39}Ar$ dating of individual micas has since shown that extraneous Ar is significant in almost all As Sifah white micas, particularly in mafic rocks [*Warren et al.*, 2011; *Smye et al.*, 2013], firmly indicating that only the youngest published Ar/Ar dates (~80 Ma) are geologically meaningful. Still, the ~110 Ma Sm-Nd garnet dates from *Gray et al.* [2004a] continue to be cited in favor of continent-ward subduction during the Early Cretaceous [e.g., *Goscombe et al.*, 2020].

3 SAMPLE DESCRIPTIONS

To understand the timing of *(U)HP* metamorphism, as well as the pre- and syn- metamorphic history of rock protoliths, we sampled several different eclogite-facies rocks that reflect the textural/chemical diversity and range of metamorphic histories recorded at As Sifah. The descriptions below are focused on samples dated by the Sm-Nd method, with subordinate descriptions for those without garnet dates. Thin-section scans of each sample can be found online at doi:10.17605/OSF.IO/CZG3P.

Sample CWO237 (23°27'30"N, 58°46'48"E) is a banded, foliated mafic eclogite, with layering defined by garnet-rich layers (1-2 mm diameter grains) with coarse-grained phengite, omphacite, blue amphibole, epidote, rutile, and hematite/ilmenite, alternating with garnet-absent, finer-grained layers of the same phases. Garnet, omphacite, and rutile are the texturally oldest phases in the sample: garnet grains are littered with fine inclusions of omphacite and larger grains of rutile + opaques, with no gradation in inclusion assemblage from core to rim (**Fig. 3a-b**). Garnet grains (and mm-scale omphacite aggregates) are locally replaced by ~100–200 μm thick rims and filled cracks with an assemblage of phengite, optically zoned blue amphibole, and epidote; the outline of these rims locally pseudomorphs the partially resorbed garnet grains (**Fig. 3c**). All of these phases are locally overprinted by chlorite ± green amphibole along garnet rims and cracks. Rare mm-scale carbonate clots (with biotite, green amphibole, and titanite-rimmed rutile) are distributed throughout the sample (**Fig. 3d**).

Sample 9125M04 (23°27’19”N, 58°46’46”E) is a granoblastic mafic eclogite that is significantly coarser-grained than CWO237 (garnet and blue amphibole grains up ~0.5 cm in diameter), and contains quartz in the peak assemblage. Garnets in this sample exhibit darker pink cores in plane-polarized light with rare chloritoid and epidote but abundant quartz and opaque inclusions, grading to lighter pink rims with similar fine-grained omphacite and rutile inclusions as in foliated eclogite CWO237 (**Fig. 3e**). Garnet cores display an internal schistosity (defined primary by opaques) that is typically at an angle to the external compositional foliation (**Fig. 3e**). Blue amphiboles display striking optical zoning and contain numerous rutile inclusions (**Fig. 3f**). This sample is significantly less retrogressed than CWO237, with chlorite and green amphibole limited to cracks in garnet; other phases were mostly unaffected.

Because we did not find zircon in either CWO237 or 9125M04, we analyzed zircon and rutile in an additional foliated mafic eclogite (CWO21; 23°27’30”N, 58°46’48”E) as well as rutile in another foliated (9125M02; 23°27’32”N, 58°46’48”E) and granoblastic eclogite (CWO23; 23°27’30”N, 58°46’48”E). CWO21 and CWO23 have been described and dated by ID-TIMS U-Pb zircon and rutile techniques elsewhere [*Warren et al.*, 2003; *Warren et al.*, 2005]. These other eclogite samples contain similar peak assemblages and textures as CWO237 and 9125M04, albeit with slightly different mineral compositions and proportions; among all eclogite samples, CWO21, 9125M04, and CWO23 contain quartz (in order of increasing quartz mode) whereas CWO237 and 9125M02 do not. Where present, zircon and rutile in all samples are found as inclusions in all major phases, including within the texturally oldest garnet-clinopyroxene assemblages [see also *Warren et al.*, 2003, their Fig. 2].

Sample 131219J02 (23°27’13”N, 58°46’47”E) is a quartz-phengite-garnet-hematite felsic tuffaceous schist (henceforth referred to as a “metafelsite”) taken from a decameter-scale horizon at outcrop. This sample is broadly similar to the one studied by *Massonne et al.* [2013] but contains no peak metamorphic ferromagnesian silicates other than garnet. 1-2 mm sized garnet grains contain inclusions of quartz, rutile, hematite, and sulfide minerals, and are highly retrogressed along chlorite and phengite-filled fractures that are texturally discordant to the phengite-defined foliation (**Fig. 3g**). The sample contains abundant accessory apatite, rutile, and zircon; apatite occurs as 0.5–1.0 mm matrix grains, whereas <200 μm-long rutile and zircon grains are dominantly found as inclusions in phengite and quartz (**Fig. 3h**) and only rarely in garnet. The sample also contains a scarce, texturally late, birefringent phase that is locally present along quartz grain boundaries that was not chemically analyzed but is most likely barite [*Massonne et al.*, 2013].

4 METHODS

4.1 Garnet EPMA maps and major-element transects

All quantitative major-element compositional data were collected using a Cameca SX-100 electron microprobe at the University of California, Santa Barbara (UCSB). Garnets were either mounted in epoxy and polished to expose central sections through each grain (CWO237) or analyzed in thin section, with the largest garnets chosen for study (9125M04, 131219J02). Natural and synthetic mineral samples were used as reference materials. Garnet X-ray maps (Ti, Ca, Mn, Mg, and Fe) were acquired on the SX-100 with an accelerating voltage of 15 kV, a beam current of 200 nA, a focused beam, and a 2–10 μm step size. Locations for quantitative garnet traverses were selected from X-ray maps or were done along prior LA-ICPMS transects. Quantitative garnet data were collected for Si, Ti, Al, Cr, Fe, Mn, Mg, Ca, Na, and K with an accelerating voltage of 15 kV, a beam current of 30 nA, a focused beam, and a 30 s dwell time. Analytical uncertainties for garnet are ≤0.5% for Si and Al, ≤1% for Fe, Ca, and Mg, ~5–10% for Mn, and significantly higher for Ti, Na, and K, each of which is close to or below detection. All garnet stoichiometry was calculated on the basis of 12 oxygens. Quantitative major-element data in **Fig. 4** are contained in **Table S1**.

4.2 Garnet LA-ICPMS trace-element transects

To measure the distribution of REE across whole garnet crystals, we performed laser-ablation measurements along the same garnet transects as analyzed by EPMA. The garnets were ablated at UCSB using a Photon Machines 193 nm excimer laser with a HelEx ablation cell, coupled to an Agilent 7700X quadrupole ICP-MS system. We used a 25 or 40 μm spot size and a laser fluence of ~1.0 J cm^{-2}. The laser was fired twice with a larger spot size to remove surface contamination and this material was allowed to wash out for ~15 seconds. Material was then continuously ablated for 200–300 shots at an 8–10 Hz repetition rate, yielding a total ablation time of ~20–30 seconds. Analyses of unknowns were bracketed by analyses of whole-rock glass BHVO-2 and doped glass NIST SRM 612 [*Pearce et al.*, 1997]; BHVO-2 was used as the primary reference material (RM) for garnet analyses because its composition is more similar to that of a silicate rock, but results using NIST SRM 612 are nearly identical. ^{28}Si was used as an internal standard to reduce elemental data collected on the 7700X, with values taken from the EPMA analysis. Measured peaks were ^{27}Al, ^{28}Si, ^{31}P, ^{44}Ca, ^{45}Sc, ^{47}Ti or ^{49}Ti, ^{52}Cr, ^{89}Y, ^{90}Zr, ^{139}La, ^{140}Ce, ^{141}Pr, ^{146}Nd, ^{147}Sm, ^{153}Eu, ^{157}Gd, ^{159}Tb, ^{163}Dy, ^{165}Ho, ^{166}Er, ^{169}Tm, ^{172}Yb, ^{175}Lu, and ^{178}Hf. Iolite plug-in version 2.21 [*Paton et al.*, 2011] for the Wavemetrics Igor Pro software was used to correct measured elemental intensities for baselines and instrumental drift, to ratio each elemental intensity to the internal standard wave, and to calculate final values for each element. Baseline intensities were fit to a spline to model the baseline during each analysis. The mean and standard error of the measured elemental concentrations were calculated after rejection of outliers more than two standard errors beyond the mean. Garnet-transect REE data are contained in **Table S2**.

4.3 Samarium-neodymium (Sm-Nd) isochron dating of garnet

Garnet separates were extracted from the <350 μm size fraction of each sample using standard mineral separation techniques (excluding heavy liquids) at UCSB, with each aliquot picked to 90-99% purity, as garnets in all samples are inclusion-rich. Two coarse garnet aliquots (>350 μm) consisting of whole garnet grains were also picked from sample CWO237, and an additional glaucophane aliquot was picked from sample 9125M04 to provide a low Sm/Nd mineral fraction. Multiple whole-rock chips were powdered with an agate mortar and pestle to make a representative whole-rock powder. Chemical dissolution, ion-exchange chromatography, and radiogenic isotope measurements were performed at Washington State University using the methods outlined in *Johnson et al.* [2018]. All isochron calculations were performed in Isoplot [*Ludwig*, 2003] using $\lambda_{Sm} = 6.54 \times 10^{-12}$ yr^{-1} [*Begemann et al.*, 2001]. ε_{Nd} was calculated using chondritic uniform reservoir (CHUR) parameters from *Bouvier et al.* [2008] ($^{143}Nd/^{144}Nd_{CHUR} = 0.512630 \pm 0.000011$, $^{147}Sm/^{144}Nd_{CHUR} = 0.1960 \pm 0.0004$); ε_{Nd} uncertainties include propagated errors on the calculated dates and measured sample Nd isotope values. Sm-Nd isotopic data, calculated dates, and ε_{Nd} are shown in **Table 1**.

4.4 Zircon U-Pb and trace-element depth profiling and spot analysis

U-Pb isotopic and trace-element data were collected simultaneously on the same zircon spots using laser-ablation split-stream (LASS) at UCSB [*Kylander-Clark et al.*, 2013]. Zircons from sample CWO21 (mafic eclogite) were taken from the same aliquot dated previously by TIMS [*Warren et al.*, 2003; *Warren et al.*, 2005]; zircons from sample 131219J02 (felsic metavolcanic) were obtained by standard mineral separation at UCSB, with zircons picked from the <350 μm size fraction. 131219J02 zircons first underwent rim-to-core depth profiling analysis, in which grains were mounted in epoxy with unpolished crystal facets facing the top of the mount; zircons from both samples were then polished to approximate central sections, imaged by cathodoluminescence (CL) using an FEI Quanta 400f FE-SEM at UCSB, and ablated. The depth profiling analytical routine was modified from the methods of *Garber et al.* [2020a]; *Garber et al.* [2020b] and is only summarized here. Zircons were analyzed in a single analytical session, using a Photon Machines 193 nm excimer laser with a HelEx ablation cell, coupled to a Nu Instruments Plasma HR multicollector inductively-coupled plasma mass spectrometer (MC-ICPMS) for U-Pb measurements, and an Agilent 7700X quadrupole ICP-MS for trace-element analyses. The laser was first fired twice to remove surface contamination and this material was allowed to wash out for 15 s; each zircon was then ablated continuously with a 20 μm spot size at 2 Hz and ~1.0 J/cm^2 for 40 shots, yielding a total of 20 seconds of analysis time. Analyses of unknowns were bracketed by analyses of matrix-matched zircon reference materials (RMs) 91500 [1062.4 ± 0.4 ID-TIMS 206Pb/238U date: *Wiedenbeck et al.*, 1995], which was used as the primary RM for U-Pb isotopes, and GJ-1 [601.7 ± 1.3 ID-TIMS 206Pb/238U date: *Jackson et al.*, 2004; *Kylander-Clark et al.*, 2013], which was used as the primary RM for trace-element measurements. Using the same parameters and methods applied to unknowns, we obtained a concordia date of 601.8±2.4 Ma for GJ-1, which is accurate to <0.1% of its reference value. For trace-element analyses, ^{90}Zr (assuming 43.14 wt. % Zr) was used as an internal standard, with measured peaks on the 7700X at ^{28}Si, ^{31}P, ^{89}Y, ^{90}Zr, ^{147}Sm, ^{153}Eu, ^{157}Gd, ^{159}Tb, ^{163}Dy, ^{165}Ho, ^{166}Er, ^{169}Tm,

^{172}Yb, ^{175}Lu, and ^{178}Hf. Iolite plug-in version 2.21 [*Paton et al.*, 2011] for the Wavemetrics Igor Pro software was used to corrected measured isotopic ratios and elemental intensities for baselines, time-dependent laser-induced inter-element fractionation, plasma-induced fractionation, and instrumental drift. Downhole fractionation was modeled using an exponential best fit. For all age and concordia calculations we used Isoplot v. 4.15 [*Ludwig*, 2003]. Rather than output each integration separately, which comes with attendant high uncertainties [see *Garber et al.*, 2020b for discussion], we selected zircon rim and core zones directly in Iolite, by identifying consistent and homogeneous portions of each analysis with respect to age and trace elements. The mean and standard error of the measured ratios of the backgrounds and peaks were calculated after rejection of outliers more than two standard errors beyond the mean. We added an additional 2% error to each ^{207}Pb/^{206}Pb and ^{238}U/^{206}Pb ratio (in quadrature) to account for variation in ablation or transport characteristics, mass-balance instabilities, or plasma loading effects, which yields a single age population for secondary RM GJ-1. Stated 2σ date uncertainties are internal – that is, they include in-run errors only – whereas the external uncertainty of this method in this laboratory (shown in brackets where noted) is ~2% [*Kylander-Clark et al.*, 2013]. All zircon depth profiling isotopic and trace-element data are available in **Table S3**.

After depth profiling (sample 131219J02 only), all zircons (CWO21 and 131219J02) were subject to laser-ablation spot analyses on polished central sections. These analyses were performed in a single session using the same instrumental set-up as for depth profiling, with a few analytical modifications (80 shots, 4 Hz laser rep rate, 25 μm spot size). Analyses of unknowns were bracketed by analyses of matrix-matched zircon RM 91500, which was used as the primary RM for U-Pb isotopes; GJ-1, which was used as the primary RM for trace-element measurements; and secondary RM Plesovice [337.13 ± 0.37 ID-TIMS 206Pb/238U date: *Sláma et al.*, 2008]. Using the same parameters and methods applied to unknowns, we obtained a concordia date of 597.6±2.0 Ma for GJ-1 and 336.1±1.2 Ma for Plesovice, which are accurate to 0.7% and 0.3% of their reference values, respectively. For trace-element analyses, ^{90}Zr (assuming 43.14 wt. % Zr) was used as an internal standard, with measured peaks on the 7700X at ^{28}Si, ^{31}P, ^{49}Ti, ^{89}Y, ^{90}Zr, ^{139}La, ^{140}Ce, ^{141}Pr, ^{146}Nd ^{147}Sm, ^{153}Eu, ^{157}Gd, ^{159}Tb, ^{163}Dy, ^{165}Ho, ^{166}Er, ^{169}Tm,

^{172}Yb, ^{175}Lu, and ^{178}Hf. Data reduction was done as for depth profiling above; only points <3% discordant were used for the final 131219J02 core age calculation. Stated 2σ date uncertainties are internal, whereas the external uncertainty of the method (shown in brackets where noted) is ~2% [*Kylander-Clark et al.*, 2013]. All zircon spot isotopic and trace-element data are available in **Table S4**.

4.5 Rutile U-Pb + TE spots (+ Zr-in-rutile T)

U-Pb and trace-element data were collected simultaneously on the same rutile spots using laser-ablation split-stream (LASS) at UCSB. All rutile grains were analyzed in thin section. Rutile grains were analyzed using the same analytical set-up as for zircon spots, but with a higher laser fluence (~1.5 J/cm^2). Analyses of unknowns were bracketed by analyses of matrix-matched rutile RM R10 (1091.6±3.5 Ma ID-TIMS ^{206}Pb/^{238}U date) [*Luvizotto et al.*, 2009] which was used as the primary RM for U-Pb isotopes, as well as rutile RMs Wodgina (2845±0.4 Ma ID-TIMS U-Pb concordia date) [*Ewing*, 2011], R9826J (381.9±1.1 Ma ID-TIMS ^{206}Pb/^{238}U date) [*Kylander-Clark et al.*, 2008], and Kragero (1087±4 Ma SHRIMP ^{207}Pb/^{206}Pb date) [*Camacho*, 1997], and whole-rock RM BHVO-2 [*Jochum et al.*, 2005], which was used as the primary RM for trace-element measurements. Using the same parameters and methods applied to unknowns, we obtained a concordia date of 2910±10 Ma for Wodgina, 394.3±3.6 Ma for R9826J, and 1106±10 Ma for Kragero, which are accurate to 2.3%, 3.2%, and 1.7% of their reference values, respectively. For trace-element analyses, ^{49}Ti (assuming 59.94 wt. % Ti) was used as an internal standard, with measured peaks on the 7700X at ^{28}Si, ^{31}P, ^{45}Sc, ^{49}Ti, ^{51}V, ^{52}Cr, ^{55}Mn, ^{57}Fe, ^{89}Y, ^{90}Zr, ^{93}Nb, ^{95}Mo, ^{178}Hf, ^{181}Ta, ^{182}W, and ^{238}U. Though data reduction proceeded mostly as for zircon spots (above), we added an additional 6% error to each ^{238}U/^{206}Pb ratio and 3% to each ^{207}Pb/^{206}Pb ratio (both in quadrature); this expanded internal uncertainty was required to make the three secondary RMs each form single age populations. Stated 2σ date uncertainties are internal; long-term standard reproducibility on rutile RMs is poorly constrained in this lab, but the secondary RM reproducibility suggests ~4% as a conservative *minimum* external uncertainty. ^{207}Pb/^{206}Pb common-Pb upper intercepts in **Fig. 8** were not anchored, i.e., they were calculated directly from the data spread along the isochron regression. All rutile isotopic and trace element data are available in **Table S5**.

5 RESULTS

5.1 Garnet EPMA maps, major-element transects, and trace-element data

Garnet grains from all samples exhibit smooth, continuous core-to-rim Mg, Mn, and Fe zoning (**Fig. 4**, top) with some diffusive Mg-rich haloes around inclusions (particularly in granoblastic eclogite 9125M04). Ca zoning is sharper and more complex in all garnets (**Fig. S1**), and typically outlines earlier euhedral to subhedral cores. Garnets in all samples are dominated by almandine (~2.0-2.5 Fe apfu) and display similar, long-wavelength, oscillatory Fe profiles (**Fig. 4**). Despite the differences between garnet inclusion assemblages in the granoblastic eclogite (91250M04) vs. the foliated eclogite (CWO237), these samples exhibit broadly similar major-element zoning profiles. Garnet zoning in metafelsite 131219J02 is unremarkable other than the presence of thin, high-Ca rims (**Fig. 4**).

The LA-ICPMS trace-element profiles are more complex and unique to each sample. Sm and Lu profiles are shown at the bottom of **Fig. 4** to demonstrate the relative behaviors of L-MREE and HREE, respectively, with the full REE patterns shown in the inset CI-normalized plots. Foliated eclogite CWO237 exhibits MREE decreases from garnet cores to rims while HREE concentrations remain more consistent, although all REE concentrations are uniformly low (<2 ppm). Garnet grains in granoblastic eclogite 9125M04 show smoothly decreasing HREE and increasing L-MREE from core to rim, evocative of Rayleigh diffusion patterns described for trace element uptake under similar metamorphic conditions [*Lapen et al.*, 2003]. Metafelsite 131219J02 exhibits the most complex zoning, with HREE-poor garnet cores grading to HREE-rich, LREE-poor annuli, while the thin, calcic rims exhibit significant enrichments in all REE. To understand the significance of the Sm-Nd dates relative to garnet growth histories for each sample, we calculated the distribution of Sm along several core-to-rim garnet transects (**Fig. 5**). Data for sample CWO237 were pooled into a single profile due to the small garnet grain size and number of data. These distributions show that granoblastic eclogite 9124M04 has the most “rim-biased” Sm concentrations, whereas the other samples contain a greater proportion of Sm in their cores; still, all analyzed garnets contain a majority of their Sm in the outer 20-30% garnet radius, while at most 25% of the total Sm is contained in garnet cores. Therefore, Sm-Nd isochron dates are likely to be averages, albeit biased toward later increments of garnet growth in each sample.

We also performed LA-ICPMS trace-element transects in garnet from foliated mafic eclogite CWO21 (**Fig. S2**) to compare with the zircon U-Pb and trace-element data collected from the same sample. The REE profiles are similar to those in granoblastic eclogite 9125M04 (**Fig. 4**), with increasing L-MREE and decreasing HREE from core to rim.

5.2 Garnet-WR Sm-Nd isotopic data

Data for three samples are contained in **Table 1** and displayed in **Fig. 6a**. Out of a total twenty-two measured aliquots, three garnet aliquots in two samples plot significantly off their respective isochrons, and are excluded as outliers. The remaining aliquots – including multiple garnet and whole-rock fractions for all samples, with an additional glaucophane aliquot in sample 9125M04 – define three stacked isochrons, representing similar ages with different initial Nd isotope compositions. Foliated eclogite CWO237 yields the highest $\varepsilon_{Nd}(t)$ (+3.8±0.4) and the youngest Sm-Nd isochron date (77.5±2.2 Ma, n=5, MSWD=0.53), in contrast to metafelsite 131219J02 with the lowest $\varepsilon_{Nd}(t)$ (-6.2±0.3) and the oldest Sm-Nd isochron date (80.9±1.3 Ma, n=7, MSWD=0.23). These endmember Sm-Nd dates just overlap within their stated uncertainties, but an unpaired, two-tailed t-test establishes their difference at the 95% confidence interval ($p<0.007$). Granoblastic eclogite 9125M04 is intermediate both isotopically ($\varepsilon_{Nd}(t)$=-0.3±0.7) and with respect to the calculated isochron date (79.0±3.2 Ma, n=7, MSWD=2.3). The average measured $^{147}Sm/^{144}Nd$ ratio for garnet from each sample correlates with these age and whole-rock isotopic differences, with progressively increasing garnet $^{147}Sm/^{144}Nd$ from foliated (youngest, +ε_{Nd}) to granoblastic to felsic eclogites (oldest, -ε_{Nd}) (**Fig. 6a**). For each sample, both pressure-digested (bombed) and tabletop whole-rock aliquots plot in nearly identical places for each sample, suggesting that there is little influence of inherited phases on the Sm-Nd isotopic results. Sm-Nd isotopic data from *Gray et al.* [2004a] are shown on **Fig. 6b** for comparison; garnet $^{147}Sm/^{144}Nd$ ratios are systematically lower than those determined in this study, and all points are bounded by the isotopic endmembers defined by our new data.

5.3 Zircon U-Pb and trace-element data

Multi-grain zircon aliquots from foliated quartz-bearing eclogite CWO21 were previously dated by ID-TIMS U-Pb [*Warren et al.*, 2003] with a concordia date of 79.06±0.32 Ma (*n*=5, MSWD=0.97). New CL images of these zircons show characteristic "soccer-ball" sector and fir-tree zoning (**Fig. 7a**) similar to previous BSE images [*Warren et al.*, 2003, their Fig. 2c]. Laser-ablation U-Pb spot data from this sample exhibit significant scatter along concordia and do not form a single population, with a lower-intercept "errorchron" date of 78.3±0.7 Ma (*n*=64, MSWD=6.1); a weighted mean date excluding outliers yields a tighter uncertainty and better MSWD but an indistinguishable date (78.3±0.7 Ma, MSWD=2.5) (**Fig. 7b-c**). Therefore, we quote the errorchron date (and its uncertainty) as an average age. Trace element abundances are extremely consistent across the entire zircon population; all grains lack a chondrite-normalized Eu anomaly and are depleted in HREE, but exhibit a Ce anomaly (**Fig. 7d**). Ti-in-zircon temperatures can be readily calculated from these zircons, as the presence of both quartz and rutile suggest unity TiO_2 and SiO_2 activities. With this assumption, the mean (1.95±0.22 ppm) or median (2.10 ppm) Ti concentrations from CWO21 zircon yield Ti-in-zircon temperatures [*Ferry and Watson*, 2007] of 612±27°C to 618±26°C (2σ external).

In contrast to the mafic zircons, the zircon images, depth profiles, and spot analyses from metafelsite 131219J02 show several age and trace-element populations. Zircon CL zoning is characterized by partly-resorbed, CL-bright, oscillatory/concentrically zoned cores with thin (≤5 μm) CL-dark zircon rims (**Fig. 7e**). Depth profiles through the rims reveal a single age- and trace-element population at 80.2±0.7 Ma (*n*=27, MSWD=1.6) (**Fig. 7f**) with the lowest Th/U (~0.01) and lowest total REE abundances in the sample. These rims exhibit a consistently positive CI-normalized REE slope from Dy to Lu in all rim analyses (**Fig. 7g**); however, we did not measure Ti and L-MREE to determine Eu±Ce anomalies or Ti-in-zircon temperatures due to exceedingly low concentrations. Spot analyses on CL-bright cores – as well as depth profiles that penetrated through the younger rims – show a second age population at 283.8±0.7 Ma (*n*=83, MSWD=1.0) (**Fig. 7f**), with higher Th/U (0.1–2), higher total REE, and consistently negative Eu/Eu* and positive Ce/Ce* (**Fig. 7g**). Sparse older zircon cores (with ~80 Ma rims) were also identified, including three grains with ~800 Ma dates, and a single grain with a concordant ~1.8 Ga date (**Fig. 7f**). These grains are not distinct in CL but they do exhibit unique trace-element characteristics. For example, the ~800 Ma population displays the most extreme Ce anomalies, the most muted Eu/Eu*, and the lowest P+Hf concentrations in the dataset, while the ~1.8 Ga grain displays the least extreme Ce anomalies (**Fig. 7g**).

5.4 Rutile U-Pb and trace-element data

Rutile U-Pb dates and most trace elements vary as a function of bulk-rock lithology (**Fig. 8**). For example, the U content of rutile progressively increases from foliated, quartz-free mafic eclogites (≤5 ppm) to the quartz-bearing foliated eclogite (5–10 ppm) to granoblastic eclogites (~10 ppm) to the endmember metafelsite (≤30 ppm), leading to progressively more precise U-Pb dates. On the other hand, while rutile grains are included in almost all other rock-forming minerals, there is no correlation between the host phase and the age or chemistry (including Zr) of the included rutile, within any rock. A plurality of rutile analytical spots sampled various microinclusions of other phases (particularly zircon); all data in **Fig. 8** and **Table S5** have been screened for inclusions, though there are still many inclusion-free spots that contain significant common Pb. Rutile U-Pb dates for the foliated mafic eclogites are imprecise due to low U and also potentially inaccurate due to Pb* loss, with horizontal arrays drawn away from the discordia lines defined by the oldest spots in each sample. As such, the mafic discordia dates in **Fig. 8a-b** (79.1±5.1 Ma, MSWD=0.43; 75.9±3.8 Ma, MSWD=0.79) are calculated from a small subset of the oldest spots (n=5 for each sample), and therefore the calculated dates only provide minimum constraints on the timing of rutile growth or U-Pb system closure. The more U-rich rutile grains in the quartz-bearing foliated eclogite also provided few inclusion-free spots, and thus yield a poorly resolved rutile U-Pb date (80±12, n=5, MSWD=2.6) (**Fig. 8c**). In contrast, the granoblastic eclogite and metafelsite data provide tighter U-Pb age constraints, with slightly younger dates for the eclogites (76.9±1.1 Ma, n=23, MSWD=0.85; 75.9±2.1 Ma; n=10, MSWD=1.3) than the metafelsite (78.7±0.9 Ma; n=28, MSWD=0.84) (**Fig. 8d-f**). Each of these latter dates forms a statistical single population [*Wendt and Carl*, 1991].

As noted for U (**Fig. 8a-f**), the clearest first-order variation in rutile trace elements is characterized by the gradation from mafic to felsic bulk compositions. However, the mean Zr concentration is uniform across the entire population (**Fig. 8g**) despite the fact that two of the eclogites lack extant quartz, which should nominally increase the equilibrium Zr concentration in rutile relative to a quartz-bearing rock at the same *P-T-a*($ZrSiO_4$) [*Ferry and Watson*, 2007]. Instead, these observations suggest that quartz was saturated in all rocks during rutile growth. Using the *Tomkins et al.* [2007] calibration of the Zr-in-rutile thermobarometer for the α-quartz field, P=20±2 kbar (suggested by eclogite phase equilibria [*Warren and Waters*, 2006]), and a(SiO_2) = a($ZrSiO_4$) = 1, the data yield a mean Zr-in-rt T=520±18°C. Using slightly higher metamorphic pressures (P=25±2 kbar) calculated from pseudosections of the metafelsite [*Massonne et al.*, 2013], the calculated temperatures are ~20°C higher (540±18°C).

6 DISCUSSION

6.1 Radiometric dates and the timing of metamorphism recorded by As Sifah eclogites

The data presented in this study support the interpretation that peak-to-early retrograde metamorphism occurred at ~81–77 Ma, variably recorded by different rocks, different metamorphic minerals, and different isotopic systems. Each result is summarized and interpreted below, and displayed graphically in **Fig. 9**.

6.1.1 Garnet

Statistically significant, five- to seven-point garnet-WR(-glaucophane) Sm-Nd isochrons define a range of garnet growth ages from 80.9±1.3 Ma (metafelsite 131219J02) to 79.0±3.2 Ma (granoblastic eclogite 9125M04) to 77.5±2.2 Ma (foliated eclogite CWO237) (**Fig. 6a**). These bulk-separate ages can be broadly interpreted as an "average" over the duration of garnet growth, but in detail, the calculated ages depend on the distribution of Sm in garnet, the garnet crystal size distributions, parent and/or daughter diffusion, and the effects of inherited phases. The latter two factors are likely insignificant here: relatively cool peak metamorphic temperatures (<550°C) preclude significant volume diffusion of either Sm or Nd over the timescales of As Sifah metamorphism [e.g., *Bloch and Ganguly*, 2015], and both tabletop and bombed whole-rock aliquots plot in the nearly the same place for all samples, suggesting whole-rock Nd isotope equilibrium and the exclusion of any inherited Nd isotopic signature. Calculation of crystal size distributions and their relationship to the timing of garnet growth are beyond the scope of this study, and are likely to be complicated by early nucleation and crystal growth processes that are now overprinted [*Carlson*, 2011]; we therefore ignore these effects.

The LA-ICPMS data show that Sm distributions are biased toward garnet rims (**Figs. 4-5**), such that the Sm-Nd dates are dominated by the outer 20-40 radial % of the bulk garnet population in each sample. Based on rock textures, garnet major-element data, and conventional thermobarometry, these garnet rims have been interpreted to record the timing of peak to early retrograde metamorphism in the As Sifah eclogites [*Warren and Waters*, 2006; *Massonne et al.*, 2013]. This interpretation is consistent with our textural observations, including **i**) omph-rt inclusions at garnet rims in the eclogites and **ii**) the growth of a late, hydrous assemblage (phg-gl-ep) associated with partial garnet rim resorption. The garnet Sm distributions are not identical in all samples, but their variation does not appear to correlate with date; for example, the granoblastic eclogite with more rim-biased Sm distributions (9125M04) yielded an older Sm-Nd date than the foliated eclogite with more core-biased Sm abundances (CWO237) (**Figs. 5-6**). Instead, the progression in Sm-Nd date correlates solely with lithology, as does ε_{Nd} and the sample-averaged garnet $^{147}Sm/^{144}Nd$ (**Fig. 6a**). These distinctions in garnet ages between more felsic and more mafic samples could arise from differences in the timing of the garnet-forming reaction in different bulk compositions, because garnet is expected to grow at lower-grade *P-T* conditions in the metafelsite [*Massonne et al.*, 2013] than the mafic eclogites [*Warren and Waters*, 2006]. These differences could also arise from kinetic factors, such as heterogeneous reaction overstepping among lithologies [*Pattison and Tinkham*, 2009]. Considering these factors, the Sm-Nd dates represent rim-biased average garnet growth ages for each lithology, and suggest that peak conditions – and the volumetric bulk of garnet growth – occurred between ~81–77 Ma.

6.1.2 Zircon

The zircon LASS data (depth profiles and spots) further bracket the timing of garnet growth, with the ages and trace elements supporting the Sm-Nd garnet-WR isochron ages. Zircon grains from quartz-bearing foliated eclogite CWO21 yield an array of dates from ~85–75 Ma, with an "average" lower-intercept date of 78.3±0.7 Ma (**Fig. 7b**). This LA-ICPMS date is within uncertainty of ID-TIMS U-Pb concordia dates on the same sample (79.06±0.32 Ma) [*Warren et al.*, 2003], as well as garnet Sm-Nd dates from both the foliated (77.5±2.2 Ma) and granoblastic eclogites (79.0±3.2 Ma). The zircon morphologies and CL zoning (**Fig. 7a**) are consistent with direct precipitation from a metamorphic fluid [*Rubatto*, 2017] as previously suggested [*Warren et al.*, 2005]. Trace elements from these zircons are nearly congruent across the entire population: significant HREE depletions in all grains (**Fig. 7d**) implicate the influence of garnet prior to or during zircon growth, and the absence of an Eu anomaly suggests consumption of any plagioclase by that time [*Rubatto and Hermann*, 2007; *Taylor et al.*, 2017]. Textural observations also clarify that zircon is associated with the peak metamorphic assemblage in each rock, with zircons grains included in garnet and omphacite and in turn containing rutile inclusions [*Warren et al.*, 2003]. The data therefore suggest that the foliated eclogite zircon U-Pb dates – both LA-ICPMS and TIMS – represent peak metamorphic crystallization ages coincident with garnet growth. However, we are skeptical that the ~10 Myr apparent range in LA-ICPMS dates is geologically significant. Rutile U-Pb systematics from the mafic eclogites are also disturbed (**Fig. 8a-c**; see below), and it is difficult to conceive of continuous, protracted precipitation of individual sector-zoned zircons from a metamorphic fluid over ~10 My (as the entire range in date is observed within single crystals). Mafic eclogite zircons with similar morphologies and sector zoning – and in similar rocks and tectonic settings – generally give punctuated dates (<1 Myr) representing discrete fluid pulses [e.g., *Rubatto and Hermann*, 2003; *Rubatto and Angiboust*, 2015; *Garber et al.*, 2020b]. As such we interpret only the average LA-ICPMS date (78.3±0.7 Ma), and not the apparent range exhibit by this sample.

We note that the calculated CWO21 Ti-in-zircon temperatures (~610–620 °C) exceed all other thermometry on the As Sifah eclogites, including the Zr-in-rutile temperatures from the same rocks in this study. The expected zircon Ti concentrations for the peak temperatures calculated from thermodynamic modelling (~550°C) are extremely low (<1 ppm); the measured Ti contents in these grains are slightly higher than this (~2 ppm), and we posit that they may be affected by rutile micro-inclusions that are difficult to filter from the data, as these are observed in BSE images of these zircon grains [*Warren et al.*, 2003]. We therefore interpret Ti-in-zircon temperatures from this sample semi-quantitatively, i.e., only to support the growth of zircon at relatively cool (~500–600°C) metamorphic temperatures, as determined by other methods.

Concordant U-Pb analyses from sector- to oscillatory-zoned zircon cores in the endmember metafelsite (131219J02; **Fig. 7e**) yield three distinct sets of dates, with rare ~1.8 Ga and ~800 Ma grains and a dominant, 283.8±0.7 Ma population. The trace elements associated with each of these populations suggest igneous rather than metamorphic zircon crystallization, particularly the significant negative Eu anomalies, elevated Th/U, and the absence of HREE depletions. The ~1.8 Ga date is common in detrital and xenocrystic igneous zircon populations throughout the Arabian plate [*Stern and Johnson*, 2010]. The ~800 Ma population matches the timing of magmatic and metamorphic activity associated with the Mirbat Granulite Complex in southwestern Oman [*Mercolli et al.*, 2006; *Bowring et al.*, 2007], which is the largest exposure of Proterozoic deep crust in eastern Arabia. These dates have been interpreted to represent the timing of continental lithosphere stabilization in E. Arabia, as there are few regional deep-crustal rocks with dates younger than 750 Ma [*Stern and Johnson*, 2010 and references therein]. The youngest zircon core population (283.8±0.7 Ma; n=83) is by far the most dominant; it is consistent with the interpretation of a tuffaceous protolith, and suggests that the older zircon populations represent magmatic xenocrysts. This date is significantly younger than the SHRIMP U-Pb zircon crystallization date of 298±3 Ma from the same metatuff horizon at As Sifah beach [*Gray et al.*, 2005a]. We cannot determine if these inter-study age differences are geologic – for example, if there were multiple discrete tuffs emplaced over ~15 My – or if they reflect analytical biases between LA-ICPMS and SHRIMP data that were collected ~15 years apart. However, though we are not aware of other similarly aged volcanics in NE Oman, zircon dates from both this study and *Gray et al.* [2005a] bracket other records of deglaciation and rifting associated with breakup of Pangaea and the opening of the Neotethys during the

Permian [*Angiolini et al.*, 2003]. For example, using brachiopod biostratigraphy of the Al-Khlata and Saiwan Formations (Haushi Group) in interior Oman, *Angiolini et al.* [2003] determined a late Sakmarian age for the initiation of rifting (~295–290 Ma), which is younger than the *Gray et al.* [2005a] dates but older than our new ages. Therefore, regardless of the distinctions in measured protolith dates, all of them demonstrate that the metafelsite marks a key stratigraphic horizon: it delineates the same pre-Permian unconformity exposed throughout the Saih Hatat and the broader Arabian rock record [e.g., *Searle et al.*, 2004].

Young zircon rims from the metafelsite (80.2±0.7 Ma) form a single age- and trace-element population with low Th/U and lower REE concentrations relative to the igneous cores – consistent with metamorphic (re)crystallization – but lack HREE depletions expected from the influence of garnet growth. This is unexpected because the Sm-Nd garnet growth age (80.9±1.3 Ma) from the same sample overlaps the U-Pb date within uncertainty. It is possible that zircon grew immediately before garnet, in which case the zircon date would bracket the start of garnet growth – or that garnet growth did not deplete the whole-rock HREE budget by the time zircon crystallized. However, it is as likely that the REE did not entirely achieve chemical equilibrium during zircon (re)crystallization, which has frequently been observed in other high-*P* altered zircons that retain a trace-element "memory" of their precursors, even in the presence of garnet [*Chen et al.*, 2010; *Štípská et al.*, 2016; *Garber et al.*, 2020b]. We therefore suggest that – like those in the eclogites – the metafelsite zircons record (re)crystallization during the growth of the peak metamorphic assemblage (garnet-phengite-quartz), which slightly preceded garnet and zircon (re)crystallization in the eclogites. The absence of any ages between ~284–80 Ma suggests that there were no zircon-forming metamorphic events during that interval.

6.1.3 Rutile

The calculated rutile U-Pb isochron dates span ~80–76 Ma, broadly matching the Sm-Nd garnet and U-Pb zircon dates. In detail, however, the most foliated eclogites yield imprecise dates with clear evidence for radiogenic Pb loss (**Fig. 8a-c**), while the granoblastic eclogites and metafelsite rutile dates are more precise (**Fig. 8d-f**) and show a similar age pattern to the garnet and zircon data, with an older metafelsite age (78.7±0.9 Ma) and younger eclogite ages (76.9±1.1 Ma; 75.9±2.1 Ma) that each form a statistical single population. There is also a progression in rutile trace-element composition across bulk compositions, particularly notable in the increasing U content from mafic to felsic rutile.

Because Pb loss can be significant in rutile at eclogite-facies conditions [*Cherniak*, 2000; *Smye et al.*, 2018], we modeled Pb diffusion to assess whether the rutile U-Pb dates are cooling or crystallization ages. Zircon fission-track dates from the As Sifah and Hulw Windows yield extremely reproducible, 66–70 Ma dates, suggesting that all samples experienced ~30°C/My cooling from eclogite-facies conditions [*Saddiqi et al.*, 2006]. Additionally, though the analyzed rutile grains are of variable sizes, all have at least one radial dimension <25 μm, which we adopt as the maximum diffusion radius. Using the *Dodson* [1973] formula for diffusive closure temperatures, a spherical grain geometry, diffusion parameters for Pb in rutile from *Cherniak* [2000], dT/dt=30°C/My, and r=10–25 μm, the effective Pb closure temperature for the As Sifah rutiles is ~560–600°C. This is higher than the Zr-in-rutile temperature determined for the same grains (520±18°C; **Fig. 8g**) as well as temperatures determined by conventional thermobarometry (~500–560°C) [*Warren and Waters*, 2006; *Massonne et al.*, 2013], nominally suggesting minimal Pb loss during cooling. This is supported by the absence of systematic differences in rutile grain size between the different lithologies, and rutile spots shifted horizontally away from concordia in the foliated eclogites (**Fig. 8a-c**) do not systematically occur in smaller grains. Critically, though there are lithology-based rutile U-Pb age differences, the entire mafic-to-felsic suite appears to have been juxtaposed since protolith emplacement: the same unit is traceable throughout the entire Hulw-As Sifah Window section (**Fig. 1**), and there are relict volcanic textures in lower-grade exposures [*Miller et al.*, 2002; *Gray et al.*, 2005a; *Warren and Miller*, 2007]. Therefore, even if the eclogites and metafelsites transformed to peak metamorphic assemblages at slightly different times – as suggested by the Sm-Nd garnet and U-Pb zircon dates – it is difficult to imagine that they would also have cooled through rutile Pb closure from peak T at different times if they were continuously juxtaposed, i.e., to yield the resolvable differences in rutile U-Pb date.

These observations suggest that the rutile U-Pb isochron dates are primarily crystallization ages with minor Pb* loss, most demonstrably in the mafic rutile grains. The rutile ages postdate Sm-Nd and U-Pb dates from the same rocks (**Fig. 9**), but this may be explained partly by systematic offsets, with far higher external uncertainties on rutile dates relative to garnet or zircon dates. The preferential mafic-rutile Pb* loss is difficult to explain with our data alone; it could imply shorter effective diffusion radii, which – if not related to macro-scale grain size – could arise from exsolved lamellae of other phases (e.g., ilmenite) or deformation-related features (e.g., dislocations). We note that mafic eclogites from As Sifah show several age disturbances in multiple isotopic systems, including **i**) extraneous Ar in phengite, particularly in mafic eclogites [e.g., *Warren et al.*, 2011], and **ii**) dispersed zircon LA-ICPMS U-Pb data along concordia (**Fig. 7b**). The Ar isotopic signatures have been shown to relate to differences in mafic vs. pelitic devolatilization during subduction [*Smye et al.*, 2013], and it is possible that the processes leading to extraneous Ar in mafic rocks also affected the Pb* systematics in rutile and zircon. In this case, the rutile U-Pb isotopic dates may reflect the timing of fluid alteration that persisted longer or more significantly in the eclogites than the metapelite.

6.1.4 Age summary

The three petrochronological datasets presented here – isotopic dates (Sm-Nd, U-Pb) and trace elements from garnet, zircon, and rutile – suggest the crystallization of the metafelsite protolith at 283.8±1.7 Ma, and the growth of peak garnet-bearing assemblages in all As Sifah beach rocks from ~81–77 Ma. There are minor lithologically controlled age variations, with the endmember metafelsite recording the earliest metamorphism in each dataset (Sm-Nd garnet: 80.9±1.3 Ma; U-Pb zircon: 80.2±0.7[±1.6] Ma; U-Pb rutile: 78.7±0.9[±2.4] Ma) and the foliated eclogites recording the most recent (Sm-Nd garnet: 77.5±2.2 Ma; U-Pb zircon: 78.3±0.7[±1.6] Ma; U-Pb rutile: imprecise and affected by Pb loss). Because the mafic and felsic endmembers appear to have been juxtaposed prior to metamorphism, these data support thermodynamic (different garnet-forming reactions) or kinetic heterogeneities (reaction overstepping). Regardless of their origin, the consistent age differences among all analyzed phases suggest that each rock transformed to peak metamorphic assemblages within a narrow time frame, before relatively rapid exhumation and cooling.

6.2 The case for a single metamorphic event in the Saih Hatat

Several authors have posited the existence of two metamorphic events in the Saih Hatat, one at ~120–110 Ma and one at ~80 Ma (**Fig. 2**). This earlier metamorphic event has also been hypothesized to result from continent-ward subduction [*Gray et al.*, 2004b; *Goscombe et al.*, 2020], which would have significant implications for the history of the Samail Ophiolite and much of the recent geological history of Oman. Critically, this tectonic hypothesis is based on which of the available geochronology of the As Sifah window is considered robust and representative, including previously measured Sm-Nd, Ar/Ar, U-Pb, and Rb-Sr dates. Below, we highlight what we consider the most significant geochronological weaknesses in the case for a ~110 Ma metamorphic event, based partly but not exclusively on our data.

1. The main line of evidence for the ~110 Ma metamorphic event is two Sm-Nd garnet-WR-leachate dates from foliated and granoblastic eclogites at 110±9 and 109±13 Ma, respectively [*Gray et al.*, 2004a]. These data are shown with our new results in **Fig. 6**. Having sampled a representative textural and lithologic range, our garnet isotopic data plot at significantly higher average $^{147}Sm/^{144}Nd$, yield more precise and statistically significant dates, and have internally consistent ε_{Nd} that varies with lithology. We detail two additional analytical issues with the existing Sm-Nd dates that are detailed in **Text S1** for an interested reader. In short, for non-geological reasons alone, we contend that the *Gray et al.* ~110 Ma Sm-Nd dates are not geologically meaningful.
2. The new zircon trace-element data demonstrate the influence of garnet during precipitation from a metamorphic fluid in the foliated eclogite samples (**Fig. 7b, d**), while the metafelsite zircon rims nominally escaped HREE resetting (**Fig. 7f-g**). However, both are within uncertainty of Sm-Nd garnet dates for the same samples (**Fig. 8**) and the trace-element observations are similar to those in other high-*P* zircons [*Chen et al.*, 2010], suggesting that the zircons grew synchronously with garnet – not during exhumation ~30 My later, as suggested by [*Gray et al.*, 2004a; *Gray et al.*, 2004b].

3. Rutile is unambiguously part of the peak, high-*P* assemblage in all the As Sifah rocks (see sample descriptions and **Fig. 3**). Because the rutile closure *T* to Pb diffusion in these rutile grains is similar to the peak metamorphic temperature (~550–600°C), any metamorphism prior to the ~81–77 Ma event should have been preserved, i.e., it would not have been totally reset, given the subsequent *T-t* history of the As Sifah eclogites. The absence of age inheritance in rutile thus supports only a single metamorphic event.
4. The other dataset that has been used to support the ~110 Ma event is Ar/Ar dating [*Miller et al.*, 1998; *Miller et al.*, 1999; *Gray et al.*, 2004b], but there are well-known issues with Ar/Ar dating in high-*P* rocks – and there have been detailed studies of grain-scale extraneous Ar in the As Sifah eclogites showing that the older ages are inaccurate and insignificant [*Warren et al.*, 2011]. These issues are particularly problematic in the more mafic lithologies due to closed-system fluid behavior [*Smye et al.*, 2013], which may also have affected the zircon and rutile U-Pb results (see above). Importantly, the Ar/Ar dates from the structurally highest, lowest-pressure nappes contain exclusively ~80 Ma phengite dates [e.g., *El-Shazly and Lanphere*, 1992]. Together, these observations suggest that the Ar/Ar dates from As Sifah eclogites do not date continental subduction in the Saih Hatat.

In summary, all demonstrably robust geochronological and geochemical data [including Sm-Nd, U-Pb, and Rb-Sr results: *El-Shazly et al.*, 2001; *Warren et al.*, 2003; *Warren et al.*, 2005, and this study] support the subduction of the Arabian continental margin to eclogite-facies conditions at ~81–77 Ma, after the crystallization of the Samail Ophiolite at ~96.2–95.0 Ma [*Rioux et al.*, 2012; *Rioux et al.*, 2013; *Rioux et al.*, 2021b] that formed the upper plate of the Saih Hatat collisional orogen. This conclusion is supported by other datasets not addressed here, including multiple structural and stratigraphic arguments that preclude such significant tectonism at 120–110 Ma [see *Searle et al.*, 2004; 2005]. Still, we emphasize that this hypothesis is untenable from a geochronological perspective alone, and that there is simply no evidence for early continent-ward subduction in Oman.

6.3 Rates of prograde subduction and retrograde exhumation

The deep, *(U)HP* subduction and exhumation of continental material – including "continental crust" in a strict sense, and continental margin rocks more broadly – has been shown to occur at a range of rates that typically correlate with the size of the subducted body and orogenic stage, such that smaller fragments subducted earlier in an orogenic event typically do so faster [e.g., Dora Maira: *Rubatto and Hermann*, 2001; *Gauthiez-Putallaz et al.*, 2016] than larger, later *(U)HP* bodies [e.g., Western Gneiss Region, Norway: *Kylander-Clark et al.*, 2008; *Kylander-Clark et al.*, 2009] [see also *Kylander-Clark et al.*, 2012]. With our new data emphasizing the late absolute timing of continental subduction and exhumation of the As Sifah eclogites beneath the Samail Ophiolite, we conclude by considering the possible rates at which this process occurred.

It is unlikely that the As Sifah-Hulw protoliths were subducted prior to the formation of the metamorphic sole in the overlying ophiolite, as these rocks record proto-subduction geotherms far hotter than those experienced by the As Sifah eclogites [*Cowan et al.*, 2014; *Soret et al.*, 2017; *Ambrose et al.*, 2021]. For example, a metapelite in the sole of the Wadi Tayin massif – which structurally overlies the Saih Hatat – experienced metamorphic conditions of 7.5±1.2 kbar, 665±32°C as late as ~93.0±0.5 Ma [*Garber et al.*, 2020a]. Additionally, there are texturally late shallow, metasediment melts in the Samail Ophiolite as young as ~95.0 Ma [*Rollinson*, 2009; *Haase et al.*, 2015; *Rollinson*, 2015; *Spencer et al.*, 2017; *Rioux et al.*, 2021a; *Rioux et al.*, 2021b]. As the ophiolite broadly represents the upper plate under which the As Sifah eclogites subducted [*Searle et al.*, 2004; *Agard et al.*, 2010a], these data represent firm bounds on the initiation of continental subduction; fortuitously, they also coincide with the stratigraphic record for downwarping of the continental margin in response to the approaching ophiolite by the Turonian [~94–90 Ma: *Robertson*, 1987]. Considering initial subduction of the margin starting at ~95.0–93.0 Ma, with material reaching peak conditions (~2.0–2.5 GPa; 60–80 km assuming lithostatic pressures) by ~81–77 Ma, and assuming a relatively shallow subduction angle [20–30°; see e.g., *Hu and Gurnis*, 2020] yields vertical sinking rates of 5±2 mm/yr and convergence rates of ~5–20 mm/yr. These rates are minima because continental subduction may have started significantly after ~95–93 Ma. However, the calculated convergence rates are less than total Arabia-Eurasia convergence at ~85–80 Ma

[~30–50 mm/yr: *Agard et al.*, 2007], compatible with the simultaneous accommodation of convergence at both Samail and Makran subduction zones at that time [*Agard et al.*, 2007]. The As Sifah sinking rates exceed those from giant *UHP* terranes such as the Western Gneiss Region [2–4 mm: *Kylander-Clark et al.*, 2009], while they match (~3–5 mm/yr: Lago di Cignana) or are slower than several *HP-UHP* Alpine exposures (>7 mm/yr: Sesia-Lanzo, Dora Maira) [*Lapen et al.*, 2003; *Rubatto et al.*, 2011; *Gauthiez-Putallaz et al.*, 2016] – suggesting that the prograde subduction of As Sifah occurred similarly to other small *HP-UHP* bodies, with continental materials dragged to mantle depths by a denser mafic slab that later detached [e.g., *Duretz et al.*, 2016].

Exhumation rates are more difficult to calculate accurately because there are few barometric constraints on the retrograde eclogite path; the only exhumation-related ages are thermochronological. However, zircon fission track dates for rocks from the As Sifah and Hulw Windows yield a consistent, reproducible 68±6 Ma (2σ) cooling age though ~260°C [*Saddiqi et al.*, 2006]; under any reasonable post-orogenic geotherm, these temperatures would have been attained at <5 kbar (≤15 km). If peak pressure conditions were attained at ~81–77 Ma, this implies exhumation rates that are similar to the sinking rates (~4–6 mm/yr). Interestingly, these time-averaged rates are slower than almost all other *(U)HP* exposures globally, regardless of size or orogenic stage [*Kylander-Clark et al.*, 2012], while other smaller *(U)HP* bodies generally exhumed ~3–5 times faster than As Sifah [*Rubatto and Hermann*, 2001]. Relatively slow exhumation of the As Sifah eclogites may have arisen from several different factors. One unique feature of As Sifah is the complete transformation of these rocks to their peak metamorphic parageneses, whereas other *(U)HP* bodies undergo limited transformation that makes them more buoyant during exhumation [e.g., *Young and Kylander-Clark*, 2015]; still, the As Sifah eclogites are bounded by abundant carbonates and calc-schists that maintain buoyancy and can accommodated significant strain even after complete transformation. More likely, there are some key tectonic differences between As Sifah and other *(U)HP* exposures; whereas the upper plate of many *(U)HP* orogens appears to undergo significant extension during exhumation [*Johnston et al.*, 2007; *Young et al.*, 2011; *Young*, 2017], the Samail Ophiolite and its cover experienced relatively little extension during emplacement [*Fournier et al.*, 2006]. At the same time, the subduction of the As Sifah rocks coincided with a significant (20–40 mm/yr) decrease in the Arabia-Eurasia convergence rate [*Agard et al.*, 2007], such that there were fewer far-field stresses driving extension of the upper plate, and – by inference – the exhumation of the subducted continental margin.

7 CONCLUSIONS

1. Sm-Nd, U-Pb, and trace-element analyses of garnet, zircon, and rutile from As Sifah eclogites (NE Oman) record ~81–77 Ma peak to early retrograde metamorphism. There are consistent lithology-based age, mineralogical, and textural differences that suggest a bulk-compositional or kinetic control on the timing of the peak assemblage in each lithology, but all the data suggest relatively punctuated transformation in each rock.
2. Protolith zircon dates for the felsic metatuff (283.3±0.7 Ma) suggest that the As Sifah eclogites mark the pre-Permian unconformity exposed throughout NE Oman, consistent with its derivation from a more distal exposure of the same rocks exposed elsewhere in the Saih Hatat.
3. There is no evidence for a ~110 Ma metamorphic episode in the As Sifah Unit; our new Sm-Nd dates show internally consistent features and cover the range of metamorphic histories preserved at As Sifah, indicating that previously published Sm-Nd dates are inaccurate. All demonstrably robust geochronology is consistent with only a single metamorphic event, in which the Arabian continental margin subducted toward the NE beneath the already emplaced Samail Ophiolite by ~81–77 Ma.
4. A comparison between other small *(U)HP* continental subduction orogens and As Sifah suggests a relatively average subduction rate, but slower exhumation for the Arabian continental margin. These values likely reflect differences in tectonic setting unique to As Sifah, including a decrease in convergence rate during subduction of the Arabian margin to mantle depths.

ACKNOWLEDGEMENTS, SAMPLES, AND DATA

This paper is dedicated to the memory of Dr. Adolphe Nicolas, who – in collaboration with Dr. Françoise Boudier – was instrumental in introducing the first and second authors to the geology of Oman, and provided incisive and thoughtful commentary as this manuscript was being assembled. We thank the Director General of Minerals, Ministry of Commerce and Industry of the Sultanate of Oman for allowing us to conduct field work in the Sultanate of Oman and facilitating its success. G. Seward is thanked for his guidance with the EPMA work at UCSB. D. Wilford and C. Knaack are thanked for their help and support with the Sm-Nd work at WSU. S. Bowring and S. Gordon are thanked for help in the field during initial sample collection with the second author. This research was supported by an ExxonMobil/Geological Society of America graduate student grant to J.M.G., National Science Foundation (USA) grants EAR-1250522 and EAR-1650407 to M.R., the University of California at Santa Barbara, and the Pennsylvania State University. The authors declare no conflicts of interest. All data supporting the conclusions in this paper (**Table 1, Table S1-S5**) are freely available online at doi:10.17605/OSF.IO/CZG3P.

FIGURE CAPTIONS

Figure 1. (**a**) Regional overview map modified from *Nicolas et al.* [2000] showing the Samail ophiolite (dark gray) and subducted continental margin rocks of the Saih Hatat (light brown). (**b**) Lithologic map of the Hulw and As Sifah windows in the Saih Hatat, modified from *Miller et al.* [2002], *Searle et al.* [2004], and *Warren and Miller* [2007]. The dominant structural feature is the “UP-LP” discontinuity (bold line), which separates “Upper Plate” rocks (dark gray) from “Lower Plate” units. A poorly-exposed but structurally necessary ductile shear zone between the Hulw and As Sifah Windows is shown in a dashed white line. Unit abbreviations: Lqms = lower-plate quartz-mica schist; Lvf = lower-plate felsic volcanic, Lvm = lower-plate mafic volcanic; Lc = lower-plate calcschist and quartz schist; Ldl = brown dolomite; Ldqms = dolomitic quartz-mica schist; Ll = Permian metacarbonate. The inset stratigraphic sketch is modified from *Miller et al.* [2002].

Figure 2. Previous geochronology from the As Sifah eclogites. Where not visible, error bars on dates are smaller than symbols. The existence of a ~110 Ma metamorphic event at As Sifah has been postulated based on two Sm-Nd garnet-WR isochron dates and an array of old white-mica $^{40}Ar/^{39}Ar$ step-heating dates, whereas U-Pb and Rb-Sr isotopic data consistently give young, ~80 Ma dates. See text for additional discussion.

Figure 3. Rock and mineral textures from foliated, quartz-free eclogite CWO237 (**a-d**), granoblastic eclogite 9125M04 (**e-f**), and metafelsite 131219J02 (**g-h**). All photomicrographs were taken on a Zeiss Axio Scan Z.1 at Penn State. Patchy shading in E-H is due to an incompletely removed carbon coat. (**a-b**) Garnet porphyroblast in plane-polarized light (PPL; A) and cross-polarized light (XPL; B) from foliated eclogite CWO237, showing the partial replacement of the primary, dry, garnet-omphacite-rutile assemblage being partially overprinted by a hydrated phengite-epidote-glaucophane paragenesis. A second chlorite + green amphible, greenschist-facies overprint is highly localized. Inclusions in all garnets from this sample are dominated by omphacite + rutile. (**c**) Pseudomorphic replacement of garnet rims in CWO237 by phengite + glaucophane. (**d**) Rare carbonate "clot" in CWO237, containing biotite, green amphibole, and titanite-rimmed rutile. (**e**) Garnet porphyroblast from granoblastic eclogite 9125M04, with an internal schistosity defined by opaque minerals at an angle to the external foliation (see inset). These garnets contain prograde quartz, chloritoid, and epidote inclusions in their cores that grade to omphacite + rutile at their rims. (**f**) Optically-zoned blue amphibolite in 9125M04 (note darker blue rims and lighter blue cores) with numerous rutile inclusions. (**g**) Highly fractured garnet in metafelsite 131219J02, wrapped by matrix phengite + quartz. Note the laser ablation spots (although this is not the same garnet displayed in **Fig. 4**). (**h**) Rutile and zircon grains included in matrix phengite from 131219J02, with radiation haloes around the zircon.

Figure 4. Garnet Mn X-ray chemical maps (top row), EPMA major-element transects (middle row), and LA-ICPMS trace-element transects (bottom row) from foliated eclogite CWO237 (left column),

granoblastic eclogite 9125M04 (middle column), and metafelsite 131219J02 (right column). For the X-ray maps, warmer colors indicate higher concentrations (scaled individually to each garnet); Ca, Fe, and Mg maps for each garnet are displayed in **Fig. S1**. The location of the quantitative transects – for both EPMA and LA-ICPMS data – are shown in green dashed lines, with the arrow defining the left-to-right progression in the subsequent plots. The insets in the bottom row show CI-normalized [*McDonough and Sun*, 1995] REE data for each sample. All major- and trace-element data shown in this plot are contained in **Tables S1-S2**.

Figure 5. Volume-normalized distribution of Sm for each LA-ICPMS garnet core-to-rim half-profile (9125M04, 131219J02) or data from several compiled transects across small garnet grains (CWO237), including but not limited to the plots in **Fig. 4**. Line colors match the lithologic classification in **Fig. 4**. All trace-element data used to construct these plots are contained in **Table S2**.

Figure 6. (**a**) Garnet-WR(-glaucophane) isochron data from this study (red, purple, and green colors as in **Figs. 4-5**). Each sample in this study yields a broadly similar date defined by 5–7 data, but with clear differences in initial $^{143}Nd/^{144}Nd$. (**b**) Zoomed-in view of the lowest $^{147}Sm/^{144}Nd$ data from this study, along with data from the same outcrop from *Gray et al.* [2004a] (orange and blue colors, with garnet, garnet leachate, and WR data). Note that **i**) the garnet aliquots in this study plot at significantly higher average $^{147}Sm/^{144}Nd$ and more precise $^{143}Nd/^{144}Nd$ than in previous work, and **ii**) that the steeper, apparently older “isochrons” from *Gray et al.* [2004a] connect data arrayed between the lithologic endmembers defined here. All data used to construct these plots are contained in **Table 1** and *Gray et al.* [2004a] (their Table 1).

Figure 7. Zircon CL, U-Pb, and trace-element results (LASS) for foliated quartz-bearing eclogite CWO21 (**a-d**) and metafelsite 131219J02 (**e-g**). (**a**) CL images of CWO21 zircons displaying “soccer-ball” like sector and fir-tree zoning. (**b**) Tera-Wasserburg concordia diagram of CWO21 zircon data, showing a

significant spread along concordia that does not form a single population; the location of each spot along the concordia curve is independent of any trace element. A weighted-mean date from the same sample (**c**) yields the same date within uncertainty, but with tighter error bounds; we therefore adopt the lower-intercept date and its uncertainty in (**b**) as a more conservative average date. (**d**) Chondrite-normalized [*McDonough and Sun*, 1995] REE patterns for CWO21 zircons, displaying relatively homogeneous patterns with a Ce anomaly but lacking a Eu anomaly. (**e**) CL images of 131219J02 zircon, displaying faint CL-dark rims on oscillatory, concentric, and/or sector-zoned CL-bright cores. (**f**) Tera-Wasserburg concordia diagram of 131219J02 zircon data, showing clearly delineated younger rims (depth profiling data) and several clusters of older zircon cores (spot data). (**g**) Chondrite-normalized REE patterns for 131219J02 zircons, with trace-element poor, young rims (blue) and trace-element rich, older cores (with colors corresponding to different U-Pb dates). All data used to construct these plots are contained in **Table S3-S4**.

Figure 8. Rutile U-Pb and trace-element results (LASS) arranged from the most mafic (**a**) to the most felsic (**f**) lithologies at As Sifah. Zr-in-rutile thermobarometry data (**g**) are shown for the same samples. All data used to construct these plots are contained in **Table S5**.

Figure 9. Summary of age results for the samples in this study (with one imprecise rutile U-Pb date omitted from the foliated eclogites). Internal 2σ uncertainties are shown in a thicker line, with systematic uncertainties shown for zircon U-Pb (2%) and rutile U-Pb (4%) in thinner lines; no additional uncertainty is added to the garnet Sm-Nd dates because the age calculation includes external errors, and mafic rutile U-Pb dates have internal uncertainties that exceed external ones. Each dataset shows a progression from older dates in the metafelsite to younger in the eclogites, while the eclogites show a decrease in rutile U-Pb age precision due to lower U and more significant Pb* loss.

Table 1. Sm-Nd data summary from As Sifah lithologies.

REFERENCES

Agard, P., L. Jolivet, B. Vrielynck, E. Burov, and P. Monié (2007), Plate acceleration: The obduction trigger?, *Earth and Planetary Science Letters*, *258*(3), 428-441, doi:https://doi.org/10.1016/j.epsl.2007.04.002.

Agard, P., A. Plunder, S. Angiboust, G. Bonnet, and J. Ruh (2018), The subduction plate interface: rock record and mechanical coupling (from long to short timescales), *Lithos*, *320-321*, 537-566, doi:https://doi.org/10.1016/j.lithos.2018.09.029.

Agard, P., M. P. Searle, G. I. Alsop, and B. Dubacq (2010a), Crustal stacking and expulsion tectonics during continental subduction: P-T deformation constraints from Oman, *Tectonics*, *29*(5), doi:https://doi.org/10.1029/2010TC002669.

Agard, P., M. P. Searle, G. I. Alsop, and B. Dubacq (2010b), Crustal stacking and expulsion tectonics during continental subduction: P-T deformation constraints from Oman, *Tectonics*, *29*(5), n/a-n/a, doi:10.1029/2010TC002669.

Agard, P., and A. Vitale-Brovarone (2013), Thermal regime of continental subduction: The record from exhumed HP–LT terranes (New Caledonia, Oman, Corsica), *Tectonophysics*, *601*, 206-215, doi:https://doi.org/10.1016/j.tecto.2013.05.011.

Agard, P., P. Yamato, M. Soret, C. Prigent, S. Guillot, A. Plunder, B. Dubacq, A. Chauvet, and P. Monié (2016), Plate interface rheological switches during subduction infancy: Control on slab penetration and metamorphic sole formation, *Earth and Planetary Science Letters*, *451*, 208-220, doi:http://dx.doi.org/10.1016/j.epsl.2016.06.054.

Ambrose, T. K., D. J. Waters, M. P. Searle, P. Gopon, and J. B. Forshaw (2021), Burial, Accretion, and Exhumation of the Metamorphic Sole of the Oman-UAE Ophiolite, *Tectonics*, *40*(4), e2020TC006392, doi:https://doi.org/10.1029/2020TC006392.

Angiolini, L., M. Balini, E. Garzanti, A. Nicora, and A. Tintori (2003), Gondwanan deglaciation and opening of Neotethys: the Al Khlata and Saiwan Formations of Interior Oman, *Palaeogeography, Palaeoclimatology, Palaeoecology*, *196*(1), 99-123, doi:https://doi.org/10.1016/S0031-0182(03)00315-8.

Begemann, F., K. R. Ludwig, G. W. Lugmair, K. Min, L. E. Nyquist, P. J. Patchett, P. R. Renne, C. Y. Shih, I. M. Villa, and R. J. Walker (2001), Call for an improved set of decay constants for geochronological use, *Geochimica et Cosmochimica Acta*, *65*(1), 111-121, doi:https://doi.org/10.1016/S0016-7037(00)00512-3.

Bloch, E., and J. Ganguly (2015), 176Lu–176Hf geochronology of garnet II: numerical simulations of the development of garnet–whole-rock 176Lu–176Hf isochrons and a new method for constraining the thermal history of metamorphic rocks, *Contributions to Mineralogy and Petrology*, *169*(2), 14, doi:10.1007/s00410-015-1115-x.

Bouvier, A., J. D. Vervoort, and P. J. Patchett (2008), The Lu–Hf and Sm–Nd isotopic composition of CHUR: Constraints from unequilibrated chondrites and implications for the bulk composition of terrestrial planets, *Earth and Planetary Science Letters*, *273*(1), 48-57, doi:http://dx.doi.org/10.1016/j.epsl.2008.06.010.

Bowring, S. A., J. P. Grotzinger, D. J. Condon, J. Ramezani, M. J. Newall, and P. A. Allen (2007), Geochronologic constraints on the chronostratigraphic framework of the Neoproterozoic Huqf Supergroup, Sultanate of Oman, *American Journal of Science*, *307*(10), 1097-1145, doi:10.2475/10.2007.01.

Camacho, A. (1997), An isotopic study of deep-crustal processes: Musgrave Block, Central Australia, 504 pp, Australian National University.

Carlson, W. D. (2011), Porphyroblast crystallization: linking processes, kinetics, and microstructures, *International Geology Review*, *53*(3-4), 406-445, doi:10.1080/00206814.2010.496184.

Chauvet, F., T. Dumont, and C. Basile (2009), Structures and timing of Permian rifting in the central Oman Mountains (Saih Hatat), *Tectonophysics*, *475*(3), 563-574, doi:https://doi.org/10.1016/j.tecto.2009.07.008.

Chen, R.-X., Y.-F. Zheng, and L. Xie (2010), Metamorphic growth and recrystallization of zircon: Distinction by simultaneous in-situ analyses of trace elements, U–Th–Pb and Lu–Hf isotopes in zircons from eclogite-facies rocks in the Sulu orogen, *Lithos*, *114*(1–2), 132-154, doi:http://dx.doi.org/10.1016/j.lithos.2009.08.006.

Cherniak, D. J. (2000), Pb diffusion in rutile, *Contributions to Mineralogy and Petrology*, *139*(2), 198-207, doi:10.1007/PL00007671.

Cowan, R. J., M. P. Searle, and D. J. Waters (2014), Structure of the metamorphic sole to the Oman Ophiolite, Sumeini Window and Wadi Tayyin: implications for ophiolite obduction processes, *Geological Society, London, Special Publications*, *392*(1), 155-175.

Dewey, J. F., and J. F. Casey (2013), The sole of an ophiolite: the Ordovician Bay of Islands Complex, Newfoundland, *Journal of the Geological Society*, *170*(5), 715-722, doi:10.1144/jgs2013-017.

Dodson, M. H. (1973), Closure temperature in cooling geochronological and petrological systems, *Contributions to Mineralogy and Petrology*, *40*(3), 259-274, doi:10.1007/BF00373790.

Duretz, T., P. Agard, P. Yamato, C. Ducassou, E. B. Burov, and T. V. Gerya (2016), Thermo-mechanical modeling of the obduction process based on the Oman Ophiolite case, *Gondwana Research*, *32*(Supplement C), 1-10, doi:https://doi.org/10.1016/j.gr.2015.02.002.

El-Shazly, A. E.-D., R. G. Coleman, and J. G. Liou (1990), Eclogites and Blueschists from Northeastern Oman: Petrology and P-T Evolution, *Journal of Petrology*, *31*(3), 629-666, doi:10.1093/petrology/31.3.629.

El-Shazly, A. E.-D. K. (2001), Are pressures for blueschists and eclogites overestimated? The case from NE Oman, *Lithos*, *56*(2–3), 231-264, doi:http://dx.doi.org/10.1016/S0024-4937(00)00050-5.

El-Shazly, A. K., M. Bröcker, B. Hacker, and A. Calvert (2001), Formation and exhumation of blueschists and eclogites from NE Oman: new perspectives from Rb–Sr and 40Ar/39Ar dating, *Journal of Metamorphic Geology*, *19*(3), 233-248, doi:https://doi.org/10.1046/j.1525-1314.2001.00309.x.

El-Shazly, A. K., and R. G. Coleman (1990), Metamorphism in the Oman Mountains in relation to the Semail ophiolite emplacement, *Geological Society, London, Special Publications*, *49*(1), 473-493, doi:10.1144/gsl.sp.1992.049.01.30.

El-Shazly, A. K., and M. A. Lanphere (1992), Two High-Pressure Metamorphic Events in NE Oman: Evidence from 40Ar/39Ar Dating and Petrological Data, *The Journal of Geology*, *100*(6), 731-751, doi:10.1086/629625.

El-Shazly, A. K., and J. G. Liou (1991), Glaucophane chloritoid-bearing assemblages from NE Oman: petrologic significance and a petrogenetic grid for high P metapelites, *Contributions to Mineralogy and Petrology*, *107*(2), 180-201, doi:10.1007/BF00310706.

El-Shazly, A. K., M. A. Worthing, and J. G. Liou (1997), Interlayered Eclogites, Blueschists and Epidote Amphibolites from NE Oman: a Record of Protolith Compositional Control and Limited Fluid Infiltration, *Journal of Petrology*, *38*(11), 1461-1487, doi:10.1093/petroj/38.11.1461.

Ewing, T. A. (2011), Hf isotope analysis and U-Pb geochronology of rutile : technique development and application to a lower crustal section (Ivrea-Verbano Zone, Italy), 385 pp, Australian National University.

Ferry, J. M., and E. B. Watson (2007), New thermodynamic models and revised calibrations for the Ti-in-zircon and Zr-in-rutile thermometers, *Contributions to Mineralogy and Petrology*, *154*(4), 429-437, doi:10.1007/s00410-007-0201-0.

Fournier, M., C. Lepvrier, P. Razin, and L. Jolivet (2006), Late Cretaceous to Paleogene post-obduction extension and subsequent Neogene compression in the Oman Mountains, *GeoArabia*, *11*(4), 17-40.

Garber, J. M., M. Rioux, A. R. C. Kylander-Clark, B. R. Hacker, J. D. Vervoort, and M. P. Searle (2020a), Petrochronology of Wadi Tayin Metamorphic Sole Metasediment, With Implications for the Thermal and Tectonic Evolution of the Samail Ophiolite (Oman/UAE), *Tectonics*, *39*(12), e2020TC006135, doi:https://doi.org/10.1029/2020TC006135.

Garber, J. M., A. J. Smye, M. D. Feineman, A. R. C. Kylander-Clark, and S. Matthews (2020b), Decoupling of zircon U–Pb and trace-element systematics driven by U diffusion in eclogite-facies zircon

(Monviso meta-ophiolite, W. Alps), *Contributions to Mineralogy and Petrology*, *175*(6), 55, doi:10.1007/s00410-020-01692-2.

Gauthiez-Putallaz, L., D. Rubatto, and J. Hermann (2016), Dating prograde fluid pulses during subduction by in situ U–Pb and oxygen isotope analysis, *Contributions to Mineralogy and Petrology*, *171*(2), 15, doi:10.1007/s00410-015-1226-4.

Glennie, K. W., M. G. Boeuf, M. H. W. Hughes-Clarke, M. Moody-Stuart, W. G. Pilaar, and B. M. Reinhardt (1973), Late Cretaceous nappes in the Oman mountains and their geologic evolution, *AAPG Bulletin*, *57*, 5-27.

Goffé, B., A. Michard, J. R. Kienast, and O. Le Mer (1988), A case of obduction-related high-pressure, low-temperature metamorphism in upper crustal nappes, Arabian continental margin, Oman: P-T paths and kinematic interpretation, *Tectonophysics*, *151*(1), 363-386, doi:https://doi.org/10.1016/0040-1951(88)90253-3.

Goscombe, B., D. A. Foster, D. Gray, D. Kelsey, and B. Wade (2020), Metamorphic response within different subduction–obduction settings preserved on the NE Arabian margin, *Gondwana Research*, *83*, 298-371, doi:https://doi.org/10.1016/j.gr.2020.02.002.

Gray, D. R., and R. T. Gregory (2000), Implications of the structure of the Wadi Tayin metamorphic sole, the Ibra-Dasir block of the Samail ophiolite, and the Saih Hatat window for late stage extensional ophiolite emplacement, Oman, *Marine Geophysical Research*, *21*(3), 211-227, doi:10.1023/a:1026772717865.

Gray, D. R., R. T. Gregory, R. A. Armstrong, I. J. Richards, and J. M. Miller (2005a), Age and Stratigraphic Relationships of Structurally Deepest Level Rocks, Oman Mountains: U/Pb SHRIMP Evidence for Late Carboniferous Neotethys Rifting, *The Journal of Geology*, *113*(6), 611-626, doi:10.1086/449325.

Gray, D. R., R. T. Gregory, and J. M. Miller (2005b), Comment on “Structural evolution, metamorphism and restoration of the Arabian continental margin, Saih Hatat region, Oman Mountains” by M.P. Searle et al, *Journal of Structural Geology*, *27*(2), 371-374, doi:https://doi.org/10.1016/j.jsg.2004.07.002.

Gray, D. R., M. Hand, J. Mawby, R. A. Armstrong, J. M. Miller, and R. T. Gregory (2004a), Sm–Nd and Zircon U–Pb ages from garnet-bearing eclogites, NE Oman: constraints on High-P metamorphism, *Earth and Planetary Science Letters*, *222*(2), 407-422, doi:https://doi.org/10.1016/j.epsl.2004.03.016.

Gray, D. R., J. M. Miller, D. A. Foster, and R. T. Gregory (2004b), Transition from subduction- to exhumation-related fabrics in glaucophane-bearing eclogites, Oman: evidence from relative fabric chronology and 40Ar/39Ar ages, *Tectonophysics*, *389*(1), 35-64, doi:https://doi.org/10.1016/j.tecto.2004.06.016.

Gregory, R. T., D. R. Gray, and J. Miller (1998), Tectonics of the Arabian margin associated with the formation and exhumation of high-pressure rocks, Sultanate of Oman, *Tectonics*, *17*(5), 657-670, doi:10.1029/98tc02206.

Haase, K. M., S. Freund, J. Koepke, F. Hauff, and M. Erdmann (2015), Melts of sediments in the mantle wedge of the Oman ophiolite, *Geology*, *43*(4), 275-278, doi:10.1130/G36451.1.

Hacker, B. R., and J. L. Mosenfelder (1996), Metamorphism and deformation along the emplacement thrust of the Samail ophiolite, Oman, *Earth and Planetary Science Letters*, *144*(3-4), 435-451.

Hu, J., and M. Gurnis (2020), Subduction Duration and Slab Dip, *Geochemistry, Geophysics, Geosystems*, *21*(4), e2019GC008862, doi:10.1029/2019gc008862.

Jackson, S. E., N. J. Pearson, W. L. Griffin, and E. A. Belousova (2004), The application of laser ablation-inductively coupled plasma-mass spectrometry to in situ U–Pb zircon geochronology, *Chemical Geology*, *211*(1), 47-69, doi:https://doi.org/10.1016/j.chemgeo.2004.06.017.

Jochum, K. P., M. Willbold, I. Raczek, B. Stoll, and K. Herwig (2005), Chemical Characterisation of the USGS Reference Glasses GSA-1G, GSC-1G, GSD-1G, GSE-1G, BCR-2G, BHVO-2G and BIR-1G Using EPMA, ID-TIMS, ID-ICP-MS and LA-ICP-MS, *Geostandards and Geoanalytical Research*, *29*(3), 285-302, doi:10.1111/j.1751-908X.2005.tb00901.x.

Johnson, T. A., J. D. Vervoort, M. J. Ramsey, J. N. Aleinikoff, and S. Southworth (2018), Constraints on the timing and duration of orogenic events by combined Lu–Hf and Sm–Nd geochronology: An example from the Grenville orogeny, *Earth and Planetary Science Letters*, *501*, 152-164, doi:https://doi.org/10.1016/j.epsl.2018.08.030.

Johnston, S. M., B. R. Hacker, and T. B. Andersen (2007), Exhuming Norwegian ultrahigh-pressure rocks: Overprinting extensional structures and the role of the Nordfjord-Sogn Detachment Zone, *Tectonics*, *26*(5), doi:https://doi.org/10.1029/2005TC001933.

Jolivet, L., B. Goffé, R. Bousquet, R. Oberhänsli, and A. Michard (1998), Detachments in high-pressure mountain belts, Tethyan examples, *Earth and Planetary Science Letters*, *160*(1), 31-47, doi:https://doi.org/10.1016/S0012-821X(98)00079-X.

Kylander-Clark, A. R. C., B. R. Hacker, and J. M. Cottle (2013), Laser-ablation split-stream ICP petrochronology, *Chemical Geology*, *345*, 99-112, doi:http://dx.doi.org/10.1016/j.chemgeo.2013.02.019.

Kylander-Clark, A. R. C., B. R. Hacker, C. M. Johnson, B. L. Beard, and N. J. Mahlen (2009), Slow subduction of a thick ultrahigh-pressure terrane, *Tectonics*, *28*(2), n/a-n/a, doi:10.1029/2007TC002251.

Kylander-Clark, A. R. C., B. R. Hacker, and C. G. Mattinson (2012), Size and exhumation rate of ultrahigh-pressure terranes linked to orogenic stage, *Earth and Planetary Science Letters*, *321-322*, 115-120, doi:https://doi.org/10.1016/j.epsl.2011.12.036.

Kylander-Clark, A. R. C., B. R. Hacker, and J. M. Mattinson (2008), Slow exhumation of UHP terranes: Titanite and rutile ages of the Western Gneiss Region, Norway, *Earth and Planetary Science Letters*, *272*(3–4), 531-540, doi:http://dx.doi.org/10.1016/j.epsl.2008.05.019.

Lapen, T. J., C. M. Johnson, L. P. Baumgartner, N. J. Mahlen, B. L. Beard, and J. M. Amato (2003), Burial rates during prograde metamorphism of an ultra-high-pressure terrane: an example from Lago di Cignana, western Alps, Italy, *Earth and Planetary Science Letters*, *215*(1), 57-72, doi:https://doi.org/10.1016/S0012-821X(03)00455-2.

Le Metour, J., D. Rabu, M. Tegyey, F. Bechennec, M. Beurrier, and M. Villey (1986), Le métamorphisme régional crétacé de faciès éclogites-schistes bleus sur la bordure omanaise de la plate-forme arabe: conséquence d'une tectogenèse précoce anté-obduction, *Comptes Rendus de l'Académie des Sciences, Série II*, *302*, 905-910.

Le Métour, J., D. Rabu, M. Tegyey, F. Béchennec, M. Beurrier, and M. Villey (1990), Subduction and obduction: two stages in the Eo-Alpine tectonometamorphic evolution of the Oman Mountains, *Geological Society, London, Special Publications*, *49*(1), 327-339, doi:10.1144/gsl.sp.1992.049.01.20.

Lippard, S. J. (1983), Cretaceous high pressure metamorphism in NE Oman and its relationship to subduction and ophiolite nappe emplacement, *Journal of the Geological Society*, *140*(1), 97-104, doi:10.1144/gsjgs.140.1.0097.

Ludwig, K. R. (2003), *Isoplot 3.00: A Geochronological Toolkit for Microsoft Excel*, Berkeley Geochronology Center Special Publication.

Luvizotto, G. L., et al. (2009), Rutile crystals as potential trace element and isotope mineral standards for microanalysis, *Chemical Geology*, *261*(3), 346-369, doi:https://doi.org/10.1016/j.chemgeo.2008.04.012.

Mann, A., and S. S. Hanna (1990), The tectonic evolution of pre-Permian rocks, Central and Southeastern Oman Mountains, *Geological Society, London, Special Publications*, *49*(1), 307-325, doi:10.1144/gsl.sp.1992.049.01.19.

Massonne, H.-J., J. Opitz, T. Theye, and S. Nasir (2013), Evolution of a very deeply subducted metasediment from As Sifah, northeastern coast of Oman, *Lithos*, *156*(Supplement C), 171-185, doi:https://doi.org/10.1016/j.lithos.2012.11.009.

McDonough, W. F., and S. s. Sun (1995), The composition of the Earth, *Chemical Geology*, *120*(3), 223-253, doi:http://dx.doi.org/10.1016/0009-2541(94)00140-4.

Mercolli, I., A. P. Briner, R. Frei, R. Schönberg, T. F. Nägler, J. Kramers, and T. Peters (2006), Lithostratigraphy and geochronology of the Neoproterozoic crystalline basement of Salalah, Dhofar, Sultanate of Oman, *Precambrian Research*, *145*(3), 182-206, doi:https://doi.org/10.1016/j.precamres.2005.12.002.

Michard, A. (1983), Les nappes de Mascate (Oman), rampe épicontinentale d'obduction à faciès schiste bleu, et la dualité apparente des ophiolites omanaises, *Sciences Géologiques, bulletins et mémoires*, 3-16.

Michard, A., F. Boudier, and B. Goffé (1991), Obduction Versus Subduction and Collision in the Oman Case and Other Tethyan Settings, paper presented at Ophiolite Genesis and Evolution of the Oceanic Lithosphere, Springer Netherlands, Dordrecht, 1991//.

Michard, A., B. Goffé, O. Saddiqi, R. Oberhänsli, and A. S. Wendt (1994), Late Cretaceous exhumation of the Oman blueschists and eclogites: a two-stage extensional mechanism, *Terra Nova*, *6*(4), 404-413, doi:https://doi.org/10.1111/j.1365-3121.1994.tb00514.x.

Miller, J. M., D. R. Gray, and R. T. Gregory (1998), Exhumation of high-pressure rocks in northeastern Oman, *Geology*, *26*(3), 235-238, doi:10.1130/0091-7613(1998)026<0235:eohpri>2.3.co;2.

Miller, J. M., D. R. Gray, and R. T. Gregory (2002), Geometry and significance of internal windows and regional isoclinal folds in northeast Saih Hatat, Sultanate of Oman, *Journal of Structural Geology*, *24*(2), 359-386, doi:https://doi.org/10.1016/S0191-8141(01)00061-X.

Miller, J. M., R. T. Gregory, D. R. Gray, and D. A. Foster (1999), Geological and geochronological constraints on the exhumation of a high-pressure metamorphic terrane, Oman, *Geological Society, London, Special Publications*, *154*(1), 241-260, doi:10.1144/gsl.sp.1999.154.01.11.

Montigny, R., O. Le Mer, R. Thuizat, and H. Whitechurch (1988), K-Ar and Ar study of metamorphic rocks associated with the Oman ophiolite: Tectonic implications, *Tectonophysics*, *151*(1-4), 345-362.

Nicolas, A., F. Boudier, B. Ildefonse, and E. Ball (2000), Accretion of Oman and United Arab Emirates ophiolite – Discussion of a new structural map, *Marine Geophysical Research*, *21*(3), 147-180, doi:10.1023/a:1026769727917.

Paton, C., J. Hellstrom, B. Paul, J. Woodhead, and J. Hergt (2011), Iolite: Freeware for the visualisation and processing of mass spectrometric data, *Journal of Analytical Atomic Spectrometry*, *26*(12), 2508-2518, doi:10.1039/C1JA10172B.

Pattison, D. R. M., and D. K. Tinkham (2009), Interplay between equilibrium and kinetics in prograde metamorphism of pelites: an example from the Nelson aureole, British Columbia, *Journal of Metamorphic Geology*, *27*(4), 249-279, doi:10.1111/j.1525-1314.2009.00816.x.

Pearce, N. J. G., W. T. Perkins, J. A. Westgate, M. P. Gorton, S. E. Jackson, C. R. Neal, and S. P. Chenery (1997), A Compilation of New and Published Major and Trace Element Data for NIST SRM 610 and NIST SRM 612 Glass Reference Materials, *Geostandards Newsletter*, *21*(1), 115-144, doi:10.1111/j.1751-908X.1997.tb00538.x.

Rioux, M., M. Benoit, I. Amri, G. Ceuleneer, J. M. Garber, M. Searle, and K. Leal (2021a), The Origin of Felsic Intrusions Within the Mantle Section of the Samail Ophiolite: Geochemical Evidence for Three Distinct Mixing and Fractionation Trends, *Journal of Geophysical Research: Solid Earth*, *126*(5), e2020JB020760, doi:https://doi.org/10.1029/2020JB020760.

Rioux, M., S. Bowring, P. Kelemen, S. Gordon, R. Miller, and F. Dudás (2013), Tectonic development of the Samail ophiolite: High-precision U-Pb zircon geochronology and Sm-Nd isotopic constraints on crustal growth and emplacement, *Journal of Geophysical Research: Solid Earth*, *118*(5), 2085-2101, doi:10.1002/jgrb.50139.

Rioux, M., S. A. Bowring, P. B. Kelemen, S. Gordon, F. Dudás, and R. Miller (2012), Rapid crustal accretion and magma assimilation in the Oman-U.A.E. ophiolite: High precision U-Pb zircon geochronology of the gabbroic crust, *Journal of Geophysical Research*, *117*, doi:10.1029/2012JB009273.

Rioux, M., J. Garber, A. Bauer, S. Bowring, M. Searle, P. Kelemen, and B. Hacker (2016), Synchronous formation of the metamorphic sole and igneous crust of the Semail ophiolite: New constraints on the tectonic evolution during ophiolite formation from high-precision U–Pb zircon geochronology, *Earth and Planetary Science Letters*, *451*, 185-195, doi:http://dx.doi.org/10.1016/j.epsl.2016.06.051.

Rioux, M., J. M. Garber, M. Searle, P. Kelemen, S. Miyashita, Y. Adachi, and S. Bowring (2021b), High-Precision U-Pb Zircon Dating of Late Magmatism in the Samail Ophiolite: A Record of Subduction Initiation, *Journal of Geophysical Research: Solid Earth*, *126*(5), e2020JB020758, doi:https://doi.org/10.1029/2020JB020758.

Robertson, A. H. F. (1987), Upper Cretaceous Muti Formation: transition of a Mesozoic nate platform to a foreland basin in the Oman Mountains, *Sedimentology*, *34*(6), 1123-1142, doi:10.1111/j.1365-3091.1987.tb00596.x.

Rollinson, H. (2009), New models for the genesis of plagiogranites in the Oman ophiolite, *Lithos*, *112*(3-4), 603-614.

Rollinson, H. (2015), Slab and sediment melting during subduction initiation: granitoid dykes from the mantle section of the Oman ophiolite, *Contributions to Mineralogy and Petrology*, *170*(3), 1-20, doi:10.1007/s00410-015-1177-9.

Rubatto, D. (2017), Zircon: The Metamorphic Mineral, *Reviews in Mineralogy and Geochemistry*, *83*(1), 261-295, doi:10.2138/rmg.2017.83.9.

Rubatto, D., and S. Angiboust (2015), Oxygen isotope record of oceanic and high-pressure metasomatism: a P–T–time–fluid path for the Monviso eclogites (Italy), *Contributions to Mineralogy and Petrology*, *170*(5), 44, doi:10.1007/s00410-015-1198-4.

Rubatto, D., and J. Hermann (2003), Zircon formation during fluid circulation in eclogites (Monviso, Western Alps): implications for Zr and Hf budget in subduction zones, *Geochimica et Cosmochimica Acta*, *67*(12), 2173-2187, doi:https://doi.org/10.1016/S0016-7037(02)01321-2.

Rubatto, D., and J. Hermann (2007), Experimental zircon/melt and zircon/garnet trace element partitioning and implications for the geochronology of crustal rocks, *Chemical Geology*, *241*(1–2), 38-61, doi:http://dx.doi.org/10.1016/j.chemgeo.2007.01.027.

Rubatto, D., and J. r. Hermann (2001), Exhumation as fast as subduction?, *Geology*, *29*(1), 3-6, doi:10.1130/0091-7613(2001)029<0003:eafas>2.0.co;2.

Rubatto, D., D. Regis, J. Hermann, K. Boston, M. Engi, M. Beltrando, and S. R. B. McAlpine (2011), Yo-yo subduction recorded by accessory minerals in the Italian Western Alps, *Nature Geoscience*, *4*, 338, doi:10.1038/ngeo1124

Saddiqi, O., A. Michard, B. Goffe, G. r. Poupeau, and R. Oberhänsli (2006), Fission-track thermochronology of the Oman Mountains continental windows, and current problems of tectonic interpretation, *Bulletin de la Société Géologique de France*, *177*(3), 127-134, doi:10.2113/gssgfbull.177.3.127.

Searle, M. P. (2007), Structural geometry, style and timing of deformation in the Hawasina Window, Al Jabal al Akhdar and Saih Hatat culminations, Oman Mountains, *GeoArabia*, *12*(2), 99-130.

Searle, M. P., and J. Cox (1999), Tectonic setting, origin, and obduction of the Oman ophiolite, *Geological Society of America Bulletin*, *111*(1), 104-122.

Searle, M. P., and J. Cox (2002), Subduction zone metamorphism during formation and emplacement of the Semail ophiolite in the Oman Mountains, *Geological Magazine*, *139*(3), 241-255.

Searle, M. P., C. J. Warren, D. J. Waters, and R. R. Parrish (2004), Structural evolution, metamorphism and restoration of the Arabian continental margin, Saih Hatat region, Oman Mountains, *Journal of Structural Geology*, *26*(3), 451-473, doi:https://doi.org/10.1016/j.jsg.2003.08.005.

Searle, M. P., C. J. Warren, D. J. Waters, and R. R. Parrish (2005), Reply to: Comment by Gray, Gregory and Miller on "Structural evolution, metamorphism and restoration of the Arabian continental margin, Saih Hatat region, Oman Mountains", *Journal of Structural Geology*, *27*(2), 375-377, doi:https://doi.org/10.1016/j.jsg.2004.07.003.

Searle, M. P., D. J. Waters, H. N. Martin, and D. C. Rex (1994), Structure and metamorphism of blueschist-eclogite facies rocks from the northeastern Oman Mountains, *Journal of the Geological Society, London*, *151*(3), 555-576.

Sláma, J., et al. (2008), Plešovice zircon — A new natural reference material for U–Pb and Hf isotopic microanalysis, *Chemical Geology*, *249*(1), 1-35, doi:https://doi.org/10.1016/j.chemgeo.2007.11.005.

Smye, A. J., J. H. Marsh, P. Vermeesch, J. M. Garber, and D. F. Stockli (2018), Applications and limitations of U-Pb thermochronology to middle and lower crustal thermal histories, *Chemical Geology*, *494*, 1-18, doi:https://doi.org/10.1016/j.chemgeo.2018.07.003.

Smye, A. J., C. J. Warren, and M. J. Bickle (2013), The signature of devolatisation: Extraneous 40Ar systematics in high-pressure metamorphic rocks, *Geochimica et Cosmochimica Acta*, *113*, 94-112, doi:http://dx.doi.org/10.1016/j.gca.2013.03.018.

Soret, M., P. Agard, B. Dubacq, A. Plunder, and P. Yamato (2017), Petrological evidence for stepwise accretion of metamorphic soles during subduction infancy (Semail ophiolite, Oman and UAE), *Journal of Metamorphic Geology*, doi:10.1111/jmg.12267.

Spencer, C. J., A. J. Cavosie, T. D. Raub, H. Rollinson, H. Jeon, M. P. Searle, J. A. Miller, B. J. McDonald, N. J. Evans, and t. E. I. M. Facility (2017), Evidence for melting mud in Earth's mantle from extreme oxygen isotope signatures in zircon, *Geology*, *45*(11), 975-978, doi:10.1130/g39402.1.

Stern, R. J., and P. Johnson (2010), Continental lithosphere of the Arabian Plate: A geologic, petrologic, and geophysical synthesis, *Earth-Science Reviews*, *101*(1), 29-67, doi:https://doi.org/10.1016/j.earscirev.2010.01.002.

Štípská, P., R. Powell, B. R. Hacker, R. Holder, and A. R. C. Kylander-Clark (2016), Uncoupled U/Pb and REE response in zircon during the transformation of eclogite to mafic and intermediate granulite (Blanský les, Bohemian Massif), *Journal of Metamorphic Geology*, *34*(6), 551-572, doi:10.1111/jmg.12193.

Taylor, R. J. M., C. Clark, S. L. Harley, A. R. C. Kylander-Clark, B. R. Hacker, and P. D. Kinny (2017), Interpreting granulite facies events through rare earth element partitioning arrays, *Journal of Metamorphic Geology*, *35*(7), 759-775, doi:10.1111/jmg.12254.

Tomkins, H. S., R. Powell, and D. J. Ellis (2007), The pressure dependence of the zirconium-in-rutile thermometer, *Journal of Metamorphic Geology*, *25*(6), 703-713, doi:10.1111/j.1525-1314.2007.00724.x.

Vitale Brovarone, A., and P. Agard (2013), True metamorphic isograds or tectonically sliced metamorphic sequence? New high-spatial resolution petrological data for the New Caledonia case study, *Contributions to Mineralogy and Petrology*, *166*(2), 451-469, doi:10.1007/s00410-013-0885-2.

Warren, C., R. Parrish, D. Waters, and M. Searle (2005), Dating the geologic history of Oman's Semail ophiolite: Insights from U-Pb geochronology, *Contributions to Mineralogy and Petrology*, *150*(4), 403-422, doi:10.1007/s00410-005-0028-5.

Warren, C. J., and J. M. Miller (2007), Structural and stratigraphic controls on the origin and tectonic history of a subducted continental margin, Oman, *Journal of Structural Geology*, *29*(3), 541-558, doi:https://doi.org/10.1016/j.jsg.2006.10.006.

Warren, C. J., R. R. Parrish, M. P. Searle, and D. J. Waters (2003), Dating the subduction of the Arabian continental margin beneath the Semail ophiolite, Oman, *Geology*, *31*(10), 889-892.

Warren, C. J., S. C. Sherlock, and S. P. Kelley (2011), Interpreting high-pressure phengite 40Ar/39Ar laserprobe ages: an example from Saih Hatat, NE Oman, *Contributions to Mineralogy and Petrology*, *161*(6), 991-1009, doi:10.1007/s00410-010-0576-1.

Warren, C. J., and D. J. Waters (2006), Oxidized eclogites and garnet-blueschists from Oman: P–T path modelling in the NCFMASHO system, *Journal of Metamorphic Geology*, *24*(9), 783-802, doi:10.1111/j.1525-1314.2006.00668.x.

Wendt, A. S., P. D'Arco, B. Goffé, and R. Oberhänsli (1993), Radial cracks around α-quartz inclusions in almandine: Constraints on the metamorphic history of the Oman mountains, *Earth and Planetary Science Letters*, *114*(4), 449-461, doi:https://doi.org/10.1016/0012-821X(93)90075-K.

Wendt, I., and C. Carl (1991), The statistical distribution of the mean squared weighted deviation, *Chemical Geology*, *86*(4), 275-285.

Wiedenbeck, M., P. AllÉ, F. Corfu, W. L. Griffin, M. Meier, F. Oberli, A. V. Quadt, J. C. Roddick, and W. Spiegel (1995), THREE NATURAL ZIRCON STANDARDS FOR U-TH-PB, LU-HF, TRACE ELEMENT AND REE ANALYSES, *Geostandards Newsletter*, *19*(1), 1-23, doi:10.1111/j.1751-908X.1995.tb00147.x.

Yamato, P., P. Agard, B. GoffÉ, V. De Andrade, O. Vidal, and L. Jolivet (2007), New, high-precision P–T estimates for Oman blueschists: implications for obduction, nappe stacking and exhumation processes, *Journal of Metamorphic Geology*, *25*(6), 657-682, doi:10.1111/j.1525-1314.2007.00722.x.

Young, D. J. (2017), Structure of the (ultra)high-pressure Western Gneiss Region, Norway: Imbrication during Caledonian continental margin subduction, *GSA Bulletin*, *130*(5-6), 926-940, doi:10.1130/b31764.1.

Young, D. J., B. R. Hacker, T. B. Andersen, and P. B. Gans (2011), Structure and ⁴⁰Ar/³⁹Ar thermochronology of an ultrahigh-pressure transition in western Norway, *Journal of the Geological Society*, *168*(4), 887-898, doi:10.1144/0016-76492010-075.

Young, D. J., and A. R. C. Kylander-Clark (2015), Does continental crust transform during eclogite facies metamorphism?, *Journal of Metamorphic Geology*, *33*(4), 331-357, doi:10.1111/jmg.12123.

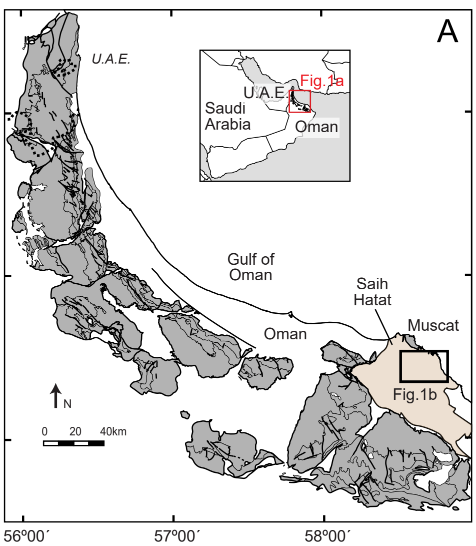

A
U.A.E.
U.A.E.
Fig.1a
Saudi Arabia
Oman
Gulf of Oman
Oman
Saih Hatat
Muscat
Fig.1b
N
0 20 40km
25°00´
24°00´
23°00´
56°00´
57°00´
58°00´

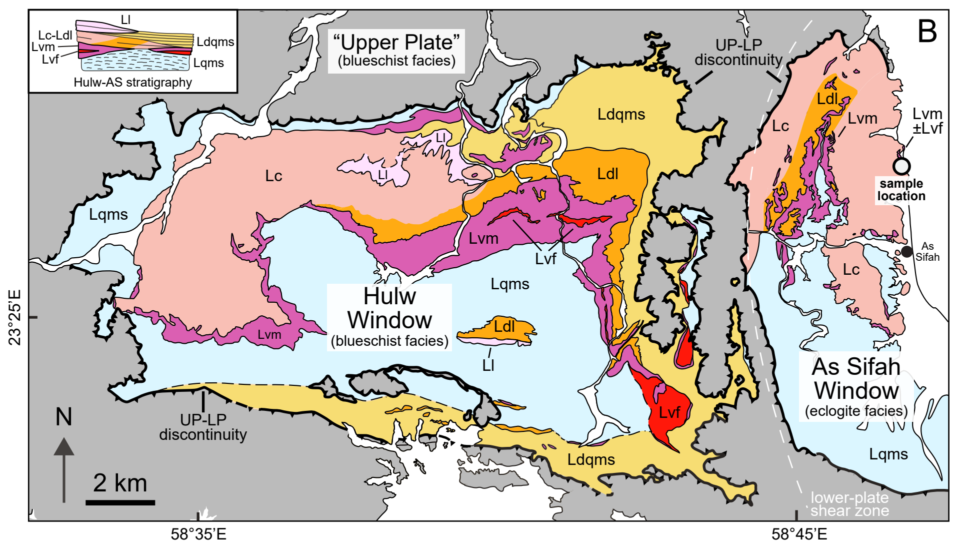

B
Ll
Lc-Ldl
Lvm
Lvf
Ldqms
Lqms
Hulw-AS stratigraphy
"Upper Plate"
(blueschist facies)
UP-LP discontinuity
Ldqms
Ldl
Lc
Ll
Lqms
Lvm
Lvf
Hulw Window
(blueschist facies)
Lqms
Ldl
Ll
Lvm
Lvf
UP-LP discontinuity
Ldqms
Lvm
±Lvf
sample location
As Sifah
Lc
As Sifah Window
(eclogite facies)
Lqms
lower-plate shear zone
N
2 km
23°25'E
58°35'E
58°45'E

Figure 1

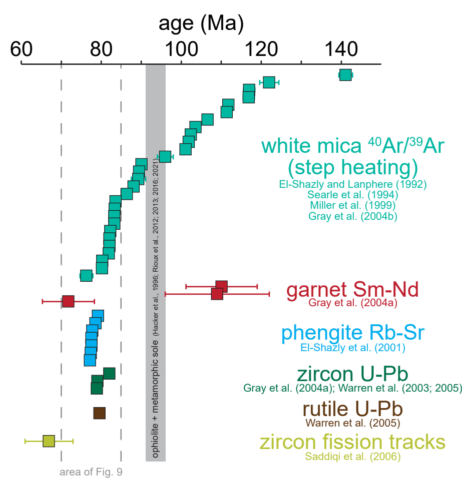

age (Ma)
60
80
100
120
140
white mica $^{40}Ar/^{39}Ar$
(step heating)
El-Shazly and Lanphere (1992)
Searle et al. (1994)
Miller et al. (1999)
Gray et al. (2004b)
ophiolite + metamorphic sole (Hacker et al., 1996; Rioux et al., 2012; 2013; 2016; 2021)
garnet Sm-Nd
Gray et al. (2004a)
phengite Rb-Sr
El-Shazly et al. (2001)
zircon U-Pb
Gray et al. (2004a); Warren et al. (2003; 2005)
rutile U-Pb
Warren et al. (2005)
zircon fission tracks
Saddiqi et al. (2006)
area of Fig. 9

Figure 2

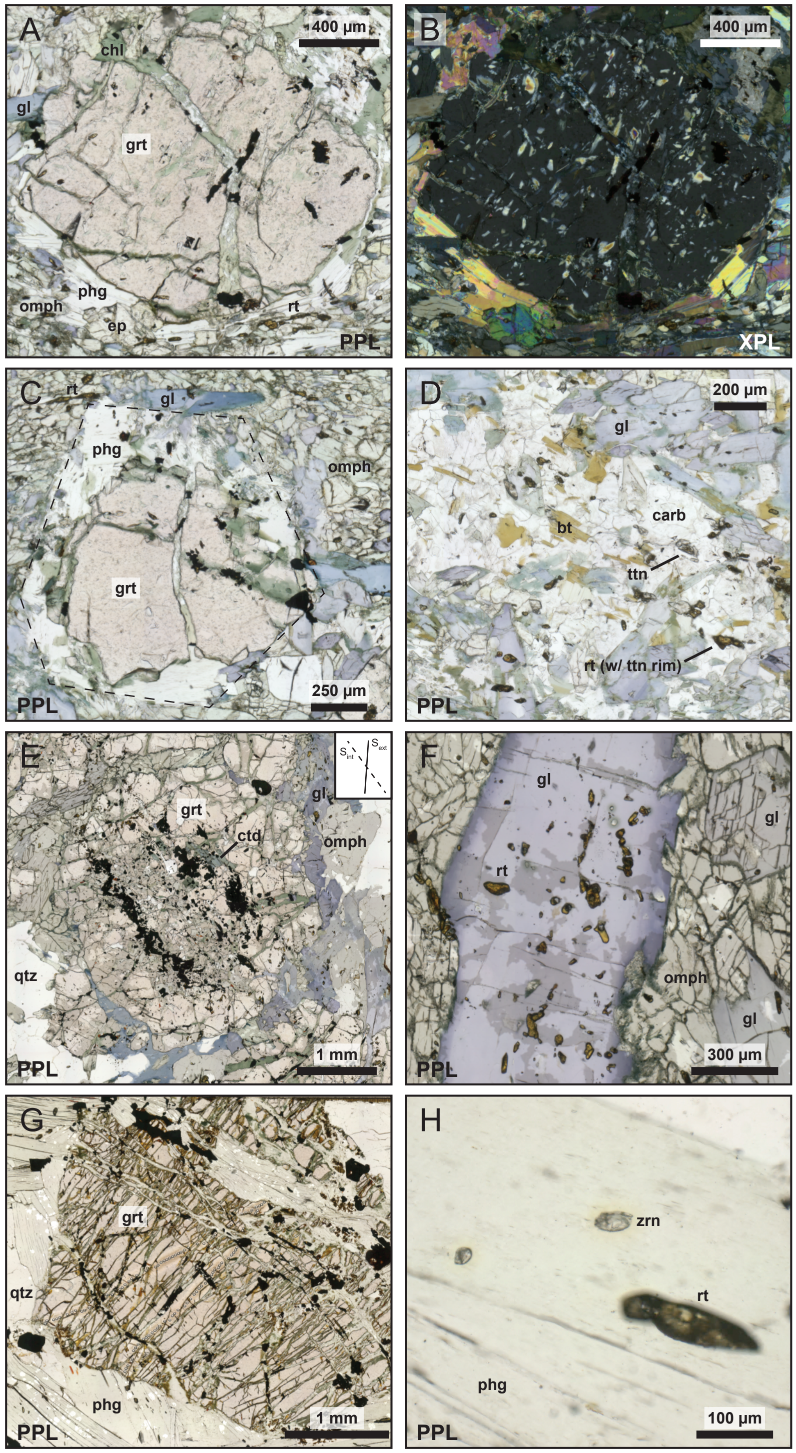

A
400 µm
chl
gl
grt
phg
omph
ep
rt
PPL
B
400 µm
XPL
C
rt
gl
phg
omph
grt
250 µm
PPL
D
200 µm
gl
carb
bt
ttn
rt (w/ ttn rim)
PPL
E
grt
ctd
gl
omph
qtz
1 mm
PPL
F
gl
rt
omph
gl
300 µm
PPL
G
grt
qtz
phg
1 mm
PPL
H
zrn
rt
phg
100 µm
PPL

Figure 3

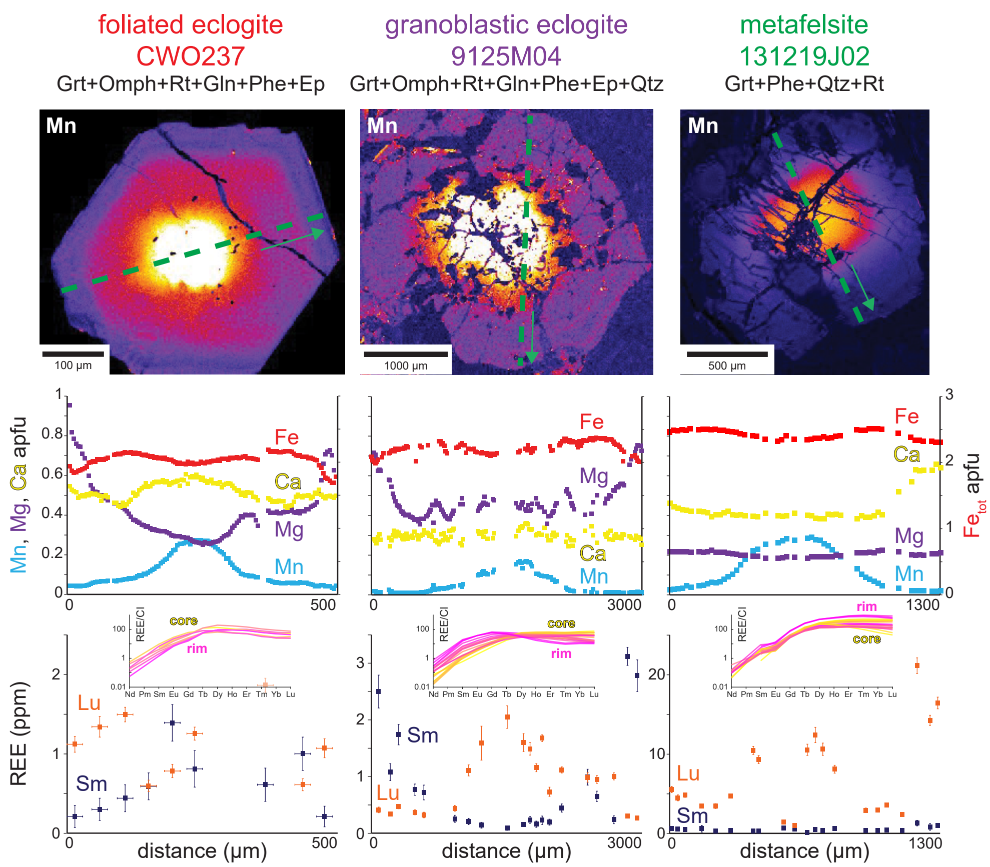

foliated eclogite
CWO237
Grt+Omph+Rt+Gln+Phe+Ep
granoblastic eclogite
9125M04
Grt+Omph+Rt+Gln+Phe+Ep+Qtz
metafelsite
131219J02
Grt+Phe+Qtz+Rt
Mn
100 μm
1000 μm
500 μm
Mn, Mg, Ca apfu
Fe
Ca
Mg
Mn
Fe_{tot} apfu
REE (ppm)
Lu
Sm
REE/CI
core
rim
Nd Pm Sm Eu Gd Tb Dy Ho Er Tm Yb Lu
distance (μm)

Figure 4

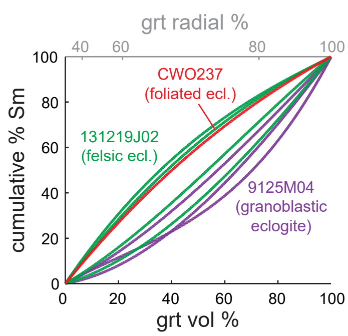

grt radial %
40
60
80
100
100
80
60
40
20
0
cumulative % Sm
CWO237
(foliated ecl.)
131219J02
(felsic ecl.)
9125M04
(granoblastic
eclogite)
0
20
40
60
80
100
grt vol %

Figure 5

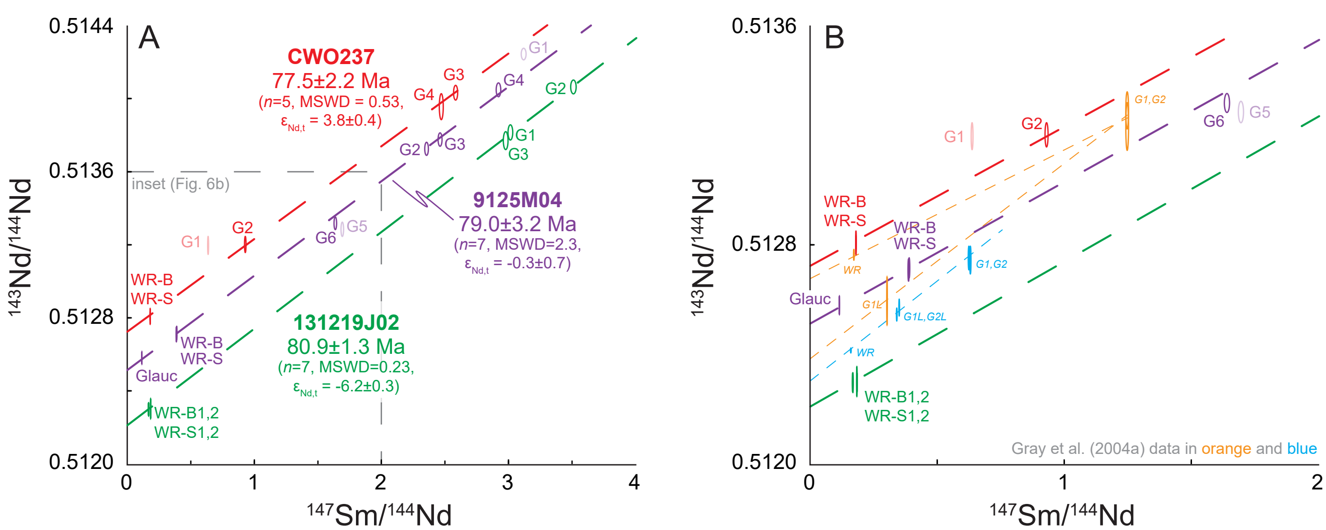
A
CWO237
77.5±2.2 Ma
(n=5, MSWD = 0.53,
εNd,t = 3.8±0.4)
9125M04
79.0±3.2 Ma
(n=7, MSWD=2.3,
εNd,t = -0.3±0.7)
131219J02
80.9±1.3 Ma
(n=7, MSWD=0.23,
εNd,t = -6.2±0.3)
inset (Fig. 6b)
143Nd/144Nd
147Sm/144Nd
B
Gray et al. (2004a) data in orange and blue

Figure 6

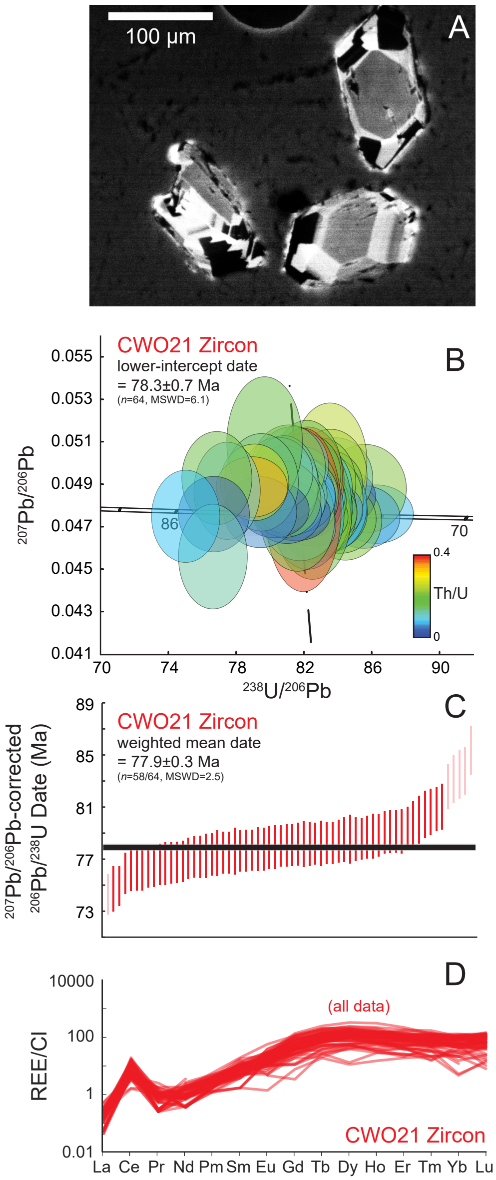

100 µm
A
250 µm
E
CWO21 Zircon
lower-intercept date
= 78.3±0.7 Ma
(n=64, MSWD=6.1)
B
131219J02 Zircon
rims = 80.2±0.7 Ma (n=27, MSWD=1.6)
cores (main pop.) = 283.8±0.7 Ma (n=83, MSWD=1.0)
F
Th/U
cores
rims
CWO21 Zircon
weighted mean date
= 77.9±0.3 Ma
(n=58/64, MSWD=2.5)
C
cores (~286 Ma)
cores (~800 Ma)
cores (~1.8 Ga)
131219J02 Zircon
G
(all data)
CWO21 Zircon
D
REE/CI
La Ce Pr Nd Pm Sm Eu Gd Tb Dy Ho Er Tm Yb Lu

Figure 7

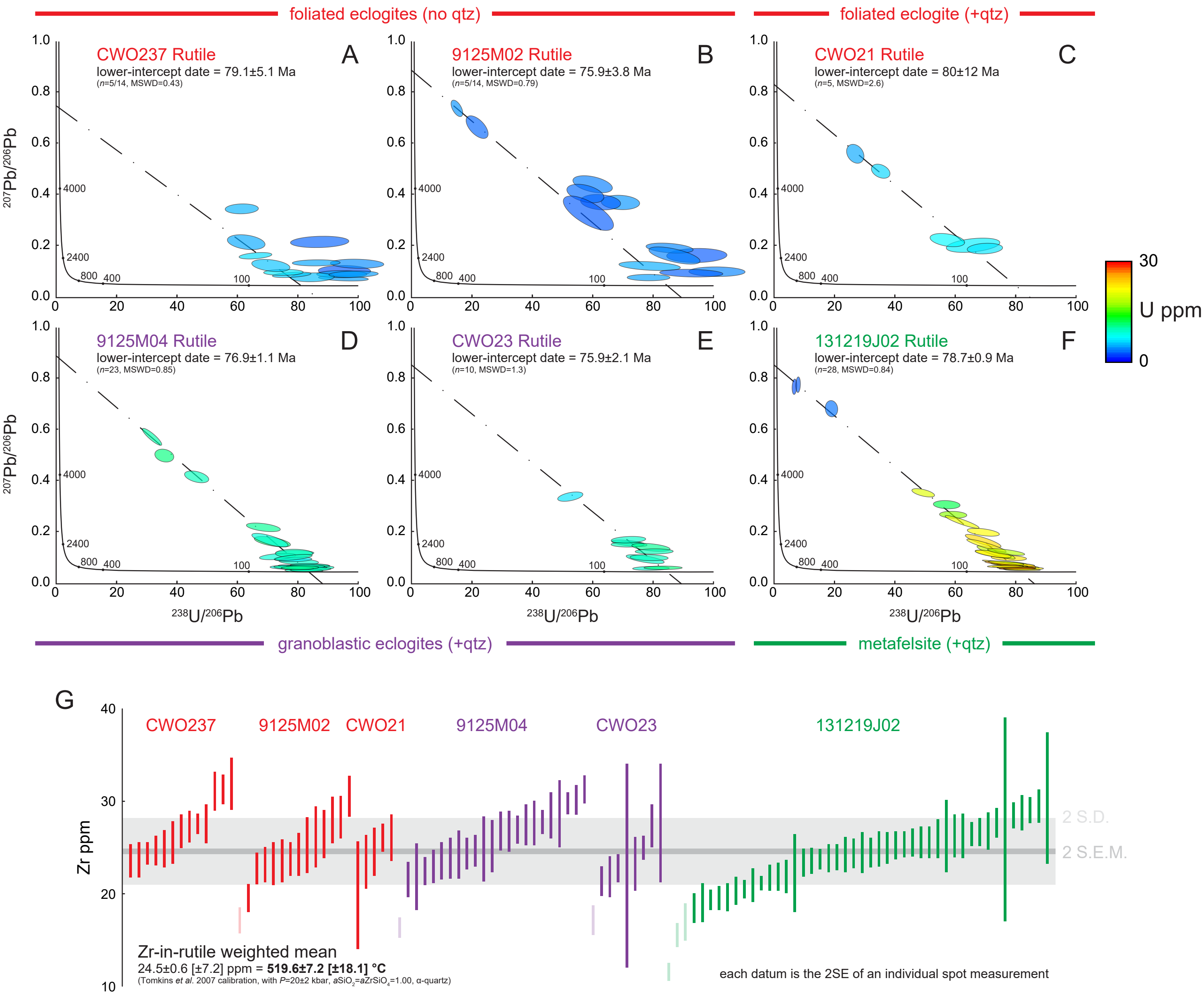

foliated eclogites (no qtz)
foliated eclogite (+qtz)
CWO237 Rutile
lower-intercept date = 79.1±5.1 Ma
(n=5/14, MSWD=0.43)
9125M02 Rutile
lower-intercept date = 75.9±3.8 Ma
(n=5/14, MSWD=0.79)
CWO21 Rutile
lower-intercept date = 80±12 Ma
(n=5, MSWD=2.6)
9125M04 Rutile
lower-intercept date = 76.9±1.1 Ma
(n=23, MSWD=0.85)
CWO23 Rutile
lower-intercept date = 75.9±2.1 Ma
(n=10, MSWD=1.3)
131219J02 Rutile
lower-intercept date = 78.7±0.9 Ma
(n=28, MSWD=0.84)
A
B
C
D
E
F
$^{207}Pb/^{206}Pb$
$^{238}U/^{206}Pb$
U ppm
granoblastic eclogites (+qtz)
metafelsite (+qtz)
G
Zr ppm
CWO237
9125M02
CWO21
9125M04
CWO23
131219J02
2 S.D.
2 S.E.M.
Zr-in-rutile weighted mean
24.5±0.6 [±7.2] ppm = 519.6±7.2 [±18.1] °C
(Tomkins et al. 2007 calibration, with P=20±2 kbar, aSiO2=aZrSiO4=1.00, α-quartz)
each datum is the 2SE of an individual spot measurement

Figure 8

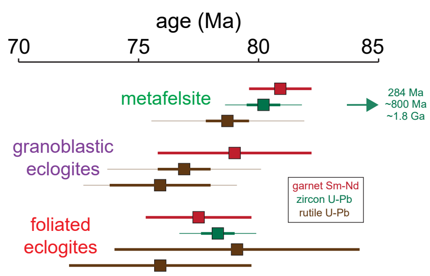

age (Ma)
70
75
80
85
metafelsite
284 Ma
~800 Ma
~1.8 Ga
granoblastic
eclogites
garnet Sm-Nd
zircon U-Pb
rutile U-Pb
foliated
eclogites

Figure 9

Table 1: Sm-Nd Data Summary

Aliquot	Description	Sm (ppm)	Nd (ppm)	$^{147}Sm/^{144}Nd$	2σ (abs)[1]	$^{143}Nd/^{144}Nd$	2σ (abs)[1]	Date[2]	εNd_i[3,4]
CWO237 (foliated eclogite)									
*G1**	*>710 µm garnet*	*0.85*	*0.81*	*0.632*	*0.003*	*0.513198*	*0.000040*		
G2	355-710 µm garnet	0.76	0.50	0.924	0.005	0.513203	0.000036		
G3	180-355 µm garnet	0.65	0.15	2.580	0.013	0.514034	0.000033		
G4	180-355 µm garnet	0.64	0.16	2.467	0.012	0.513958	0.000058		
WR-B	bombed whole rock	3.34	11.49	0.176	0.001	0.512819	0.000027		
WR-S	tabletop whole rock	3.33	11.46	0.176	0.001	0.512801	0.000028		
								77.5±2.2 Ma	**-3.8±0.4**
9125M04 (granoblastic eclogite)									
*G1**	*90-355 µm garnet*	*0.82*	*0.16*	*3.115*	*0.016*	*0.514246*	*0.000026*		
G2	90-355 µm garnet	1.53	0.39	2.352	0.012	0.513727	0.000029		
G3	90-355 µm garnet	1.93	0.47	2.458	0.012	0.513778	0.000030		
G4	90-355 µm garnet	1.50	0.31	2.917	0.015	0.514050	0.000031		
*G5**	*90-355 µm garnet*	*1.22*	*0.44*	*1.688*	*0.008*	*0.513286*	*0.000032*		
G6	90-355 µm garnet	1.65	0.61	1.633	0.008	0.513319	0.000028		
Glauc	355-710 µm glaucophane	1.14	6.25	0.110	0.001	0.512582	0.000027		
WR-B	bombed whole rock	1.86	2.95	0.382	0.002	0.512710	0.000033		
WR-S	tabletop whole rock	1.90	2.99	0.385	0.002	0.512718	0.000030		
								79.0±3.2 Ma	**-0.3±0.7**
131219J02 (metafelsite)									
G1	90-355 µm garnet	1.68	0.34	3.012	0.015	0.513817	0.000034		
G2	90-355 µm garnet	1.67	0.29	3.508	0.018	0.514066	0.000031		
G3	90-355 µm garnet	1.59	0.32	2.974	0.015	0.513772	0.000040		
WR-B1	bombed whole rock	2.10	7.74	0.164	0.001	0.512300	0.000029		
WR-B2	bombed whole rock	2.96	9.97	0.179	0.001	0.512304	0.000044		
WR-S1	tabletop whole rock	3.02	10.16	0.180	0.001	0.512301	0.000028		
WR-S2	tabletop whole rock	2.18	8.13	0.162	0.001	0.512301	0.000028		
								80.9±1.3 Ma	**-6.2±0.3**

[1]in-run uncertainties only

[2]age calculation includes propagated systematic uncertainties on all ratios

[3]calculated with CHUR parameters from Bouvier et al. (2008): $^{143}Nd/^{144}Nd$ = 0.512630±0.000011, $^{147}Sm/^{144}Nd$ = 0.1960±0.0004

[4]uncertainties include error on the calculated date and $^{143}Nd/^{144}Nd_i$

*excluded from age calculation